

University of New Mexico

UNM Digital Repository

Mechanical Engineering ETDs

Engineering ETDs

11-30-1987

Investigation Of The Excessive Bending Stiffness Of The Four Node Plane Stress/Plane Strain Quadrilateral Finite Element

William Lee Hacker

Follow this and additional works at: https://digitalrepository.unm.edu/me_etds



Part of the [Mechanical Engineering Commons](#)

THE UNIVERSITY OF NEW MEXICO
ALBUQUERQUE, NEW MEXICO 87131

POLICY ON USE OF THESES AND DISSERTATIONS

Unpublished theses and dissertations accepted for master's and doctor's degrees and deposited in the University of New Mexico Library are open to the public for inspection and reference work. *They are to be used only with due regard to the rights of the authors.* The work of other authors should always be given full credit. Avoid quoting in amounts, over and beyond scholarly needs, such as might impair or destroy the property rights and financial benefits of another author.

To afford reasonable safeguards to authors, and consistent with the above principles, anyone quoting from theses and dissertations must observe the following conditions:

1. Direct quotations during the first two years after completion may be made only with the written permission of the author.
2. After a lapse of two years, theses and dissertations may be quoted without specific prior permission in works of original scholarship provided appropriate credit is given in the case of each quotation.
3. Quotations that are complete units in themselves (e.g., complete chapters or sections) in whatever form they may be reproduced and quotations of whatever length presented as primary material for their own sake (as in anthologies or books of readings) ALWAYS require consent of the authors.
4. The quoting author is responsible for determining "fair use" of material he uses.

This thesis/dissertation by William Lee Hacker has been used by the following persons whose signatures attest their acceptance of the above conditions. (A library which borrows this thesis/dissertation for use by its patrons is expected to secure the signature of each user.)

NAME AND ADDRESS

DATE

_____	_____
_____	_____
_____	_____
_____	_____
_____	_____

William Lee Hacker
Candidate

Mechanical Engineering
Department

This thesis is approved, and it is acceptable in quality
and form for publication on microfilm:

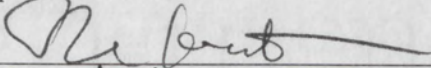
Approved by the Thesis Committee:

Howard L. Schreyer, Chairperson

C. Randall Human

Samuel W. Ky

Accepted:


Asst. Dean, Graduate School

November 30, 1987
Date

INVESTIGATION OF THE EXCESSIVE BENDING STIFFNESS
OF THE FOUR NODE PLANE STRESS/PLANE STRAIN
QUADRILATERAL FINITE ELEMENT

By

WILLIAM LEE HACKER

B.S., New Mexico State University, 1984

THESIS

Submitted in Partial Fulfillment of the
Requirements for the Degree of

Master of Science in Mechanical Engineering

The University of New Mexico
Albuquerque, New Mexico

December, 1987

ACKNOWLEDGEMENTS

This thesis was prepared under the supervision of Dr. H.L. Schreyer. I am indebted to Dr. Schreyer for his assistance, guidance, and encouragement throughout this project. I am also grateful for the helpful insight provided by Dr. S.W. Key and his review of this work.

INVESTIGATION OF THE EXCESSIVE BENDING STIFFNESS
OF THE FOUR NODE PLANE STRESS/PLANE STRAIN
QUADRILATERAL FINITE ELEMENT

By
WILLIAM LEE HACKER

ABSTRACT OF THESIS

Submitted in Partial Fulfillment of the
Requirements for the Degree of
Master of Science in Mechanical Engineering

The University of New Mexico
Albuquerque, New Mexico

December, 1987

INVESTIGATION OF THE EXCESSIVE BENDING STIFFNESS
OF THE FOUR NODE PLANE STRESS/PLANE STRAIN
QUADRILATERAL FINITE ELEMENT

William Lee Hacker

B.S. Mechanical Engineering, New Mexico State University, 1984

M.S. Mechanical Engineering, University of New Mexico, 1987

An eigenvalue-eigenvector approach is taken to study the details of the causes of and remedies for the overly stiff behavior exhibited by this element. The exact functional variation of the eigenpairs with element aspect ratio and material properties are derived for rectangular elements. These analytic expressions for the eigenpairs have not previously appeared in the literature. It is then shown that only the eigenvalues of the two flexure modes are decreased by the lower integration rules that are often applied, thereby causing a more flexible response. Knowing the variation in the eigenvalues with the various integrations then allows the element to be formulated in terms of the stabilization matrix. With this formulation, finite element simulations of a cantilever beam were run in which several methods of setting the flexure mode eigenvalues were used. The ability of each method to provide more flexible displacements for three aspect ratios and two Poisson ratios were compared.

The results show that decreasing the flexure eigenvalues works well for systems whose response is dominated by the flexure modes. This is the case when the beam thickness is modelled by only a few elements. However, care must be taken to ensure that monotonic convergence is not lost. But as the number of elements used through the beam thickness increases, the contribution of the flexure modes to the overall system response decreases and so does the effect of changing the element's flexure mode eigenvalues.

TABLE OF CONTENTS

	Page
I. Introduction	1
II. Problem Development	3
II.A. Derivation of the Element Stiffness Matrix	3
II.B. Numerical Integration	11
II.C. Detailed Description of the Problem	15
III. Eigenvalue-Eigenvector Interpretation of the Problem	21
IV. Stabilization Matrix	33
V. Numerical Results	37
VI. Conclusions	48
References	50

LIST OF FIGURES

Figure	Page
1. Element Mapping	8
2. Components of Fully Integrated Element Stiffness Matrix	10
3. Components of a 2×1 Integration of the Element Stiffness Matrix ...	12
4. Components of a 1×2 Integration of the Element Stiffness Matrix ...	13
5. Components of a One-Point Integration of the Element Stiffness Matrix	14
6. Components of Element Stiffness Matrix Evaluated by Reduced-Selective Integration	19
7. Mode Shapes	24
8. Shear, Stretching, and Extension Mode Eigenvalues	26
9. Flexure Mode Eigenvalues	27
10. Flexure Mode Eigenvalues for Full and 2×1 Integrations	29
11. Flexure Mode Eigenvalues for Full and 1×2 Integrations	30
12. Flexure Mode Eigenvalues for Full and Reduced-Selective Integrations	32
13. Components of Element Stabilization Matrix	35
14. Cantilever Beam Problem	37
15. Normalized Tip Displacements, $\frac{a}{b} = 1, \nu = 0.25$	40
16. Normalized Tip Displacements, $\frac{a}{b} = 2.5, \nu = 0.25$	41
17. Normalized Tip Displacements, $\frac{a}{b} = 5, \nu = 0.25$	42
18. Normalized Tip Displacements, $\frac{a}{b} = 1, \nu = 0.45$	43
19. Normalized Tip Displacements, $\frac{a}{b} = 2.5, \nu = 0.45$	44
20. Normalized Tip Displacements, $\frac{a}{b} = 5, \nu = 0.45$	45

LIST OF TABLES

Table	Page
1. Flexure Mode Eigenvalues for Various Integrations	28
2. Flexure Mode Eigenvalues for Full and Reduced-Selective Integrations	31
3. Additional Stiffness Parameters	47

I. Introduction

The development of the finite element method as a means of numerically simulating the response of a physical system to various loadings coupled with the advances in computer technology have led to solutions of a large number of engineering problems that would not otherwise have been available. But, as with any other method, the finite element method has its own set of drawbacks. The performance of certain elements, although very good under ideal circumstances, has been shown (MacNeal and Harder, 1985) to deteriorate rapidly with common variations in loadings, element geometries, problem geometries, and material properties. The four node plane stress/strain quadrilateral finite element has received considerable attention with regard to the excessively stiff behavior it exhibits in bending and for nearly incompressible materials. The response of the element has also been seen to worsen with increasing element aspect ratio. It has been the subject of this study to investigate the causes and remedies for the poor bending response of the four node quadrilateral with variations in element aspect ratio and material properties. The four node quadrilateral element was chosen because of its relative simplicity, for then the causes of the poor behavior are less likely to be obscured by the mathematical details required to describe the element.

For the case of materials that have a Poisson's ratio approaching 0.5 (incompressible), the four node quadrilateral as well as other elements have been seen to yield poor results. The cause of this behavior is that various terms in the stiffness matrix approach infinity as the material becomes more incompressible. To remedy this condition, Zienkiewicz (1977) suggests applying a lower order integration rule to offset the excess stiffness that arises. The stiffness matrix is thus dominated by the more important distortional energy terms and the idea of reduced-selective integration has emerged.

Reduced integration has also been applied to alleviate the excess stiffness of the

element for other material conditions. This approach is generally used in dynamic formulations that employ explicit time integrators not only because it "relaxes" the element but also provides an efficient numerical algorithm (the use of one quadrature point instead of four to obtain the stiffness terms for the quadrilateral element). However, while underintegration is applied to only part of the formulation for incompressible materials, here the entire element is underintegrated giving rise to singularities. These show up as mesh instabilities in dynamic problems and are often referred to as hourglassing or hourglass modes. It has been shown (Jacquotte and Oden, 1984) that the hourglass modes reside in the kernel of the discretized operator of the governing differential equation along with the rigid body modes.

Many methods have been used to combat the hourglass modes as they can oscillate (sometimes without bound) and obscure the solution to the problem. Flanagan and Belytschko (1981) discussed the use of anti-hourglass viscosities and stiffnesses. Schulz (1985) proposed using a Taylor series expansion of the stress along with retention of additional terms beyond the usual constant stress term. Also, Belytschko *et al.* (1984) forwarded the concept of a stabilization matrix which is some fraction of the difference between the fully integrated and underintegrated stiffness matrix.

This thesis presents the details that describe the stiff response of the element under the conditions mentioned above, as well as why the various underintegration schemes work. An eigenvalue-eigenvector interpretation of the problem is given as these eigenpairs are measures of the stiffness of the element. The exact functional variation of the eigenpairs with aspect ratio and material properties (which has not as yet appeared in the literature) are derived for rectangular elements. Also, the contribution of certain eigenpairs to the stabilization matrix is discussed and the concept is applied to a static cantilever beam problem. Using this formulation, two methods of choosing the eigenvalues that determine the matrix are presented as a means of obtaining a more flexible response.

II. Problem Development

II.A. Derivation of the Element Stiffness Matrix

In order to discuss the various problems associated with the element and their remedies, the stiffness matrix of the element must first be derived.

The governing equations for the static elasticity problem are the equation of equilibrium, the strain-displacement equation, the constitutive relationship, and the boundary conditions. The equation of equilibrium is

$$\mathbf{T} \cdot \nabla + \rho \mathbf{b} = 0, \quad (2.1)$$

where \mathbf{T} denotes the Cauchy stress tensor, \mathbf{b} is a body force vector, ρ is the mass density, and ∇ is the del operator which involves partial differentiation with respect to the rectangular cartesian coordinates. The strain displacement relation is (for infinitesimal deformation)

$$\mathbf{E} = \frac{1}{2}(\mathbf{u} \nabla + \nabla \mathbf{u}), \quad (2.2)$$

where \mathbf{E} is the strain tensor, and \mathbf{u} is the displacement vector. The stress-strain constitutive relationship is

$$\mathbf{T} = \mathbf{C} : \mathbf{E}, \quad (2.3)$$

where \mathbf{C} is the fourth order elasticity tensor.

A general form of the boundary conditions is

$$\mathbf{A} \cdot \mathbf{t} + \mathbf{B} \cdot \mathbf{u} = \mathbf{g} \text{ on } \partial R \quad (2.4)$$

where \mathbf{t} is the traction vector, \mathbf{u} is the displacement, \mathbf{A} and \mathbf{B} are prescribed tensors, and \mathbf{g} is a prescribed vector. ∂R is the boundary of the region being analyzed. It is more common, however, for boundary conditions in engineering problems to be either applied traction or applied displacement conditions on separate regions of the boundary of the problem. These can be described as

$$\mathbf{t} = \mathbf{t}^* \text{ on } \partial R_t \quad (2.5)$$

$$\mathbf{u} = \mathbf{u}^* \text{ on } \partial R_u \quad (2.6)$$

with

$$\partial R_t + \partial R_u = \partial R \quad (2.7)$$

where \mathbf{t}^* is the applied traction vector and \mathbf{u}^* describes the displacement boundary conditions. Then since the traction is a linear transformation of the unit vector normal to the boundary, Equation (2.5) becomes

$$\mathbf{T} \cdot \mathbf{n} = \mathbf{t}^* \text{ on } \partial R_t. \quad (2.8)$$

The applied traction has thus become a stress boundary condition. The problem is now completely specified with the boundary conditions and the problem geometry.

The problem can then be solved directly (strong formulation) or indirectly in the sense of weighted averages (weak formulation). To do the latter, a weighting vector \mathbf{w} is dotted with the equation of equilibrium and the stress boundary condition and integrated over the volume and boundary of the domain, respectively,

$$\int_R \mathbf{w} \cdot (\mathbf{T} \cdot \nabla + \rho \mathbf{b}) dV - \int_{\partial R_t} \mathbf{w} \cdot (\mathbf{T} \cdot \mathbf{n} - \mathbf{t}^*) dA = 0, \forall \mathbf{w}. \quad (2.9)$$

The vector \mathbf{w} is arbitrary except for the requirements that \mathbf{w} is zero on ∂R_u and that \mathbf{w} does not cause any of the integrands to become infinite. The first term of the first integral in Equation (2.9) can be rewritten as

$$\int_R \mathbf{w} \cdot (\mathbf{T} \cdot \nabla) dV = \int_R (\mathbf{w} \cdot \mathbf{T}) \cdot \nabla dV - \int_R (\mathbf{w} \nabla) : \mathbf{T} dV \quad (2.10)$$

Then by using the divergence theorem on the first term on the right hand side, Equation (2.10) becomes

$$\int_R \mathbf{w} \cdot (\mathbf{T} \cdot \nabla) dV = \int_{\partial R_t} \mathbf{w} \cdot \mathbf{T} \cdot \mathbf{n} dA - \int_R (\mathbf{w} \nabla) : \mathbf{T} dV \quad (2.11)$$

where use has been made of the fact that the integrand is zero on ∂R_u . Now combine Equation (2.2) with Equation (2.3), and substitute the result into the last term of Equation (2.11) to obtain

$$\int_R (\mathbf{w} \nabla) : \mathbf{T} dV = \int_R (\mathbf{w} \nabla) : \mathbf{C} : (\nabla \mathbf{u}) dV \quad (2.12)$$

because the part of the elasticity tensor that is dotted with the displacement gradients is symmetric. Then by combining Equations (2.9) through (2.12) and taking the body force to be zero, the following is the weak formulation of the problem

$$\int_R (\mathbf{w} \nabla) : \mathbf{C} : (\nabla \mathbf{u}) dV = \int_{\partial R_t} \mathbf{w} \cdot \mathbf{t}^* dA \quad \forall \mathbf{w} \in C^0 \quad (2.13)$$

where C^0 denotes that \mathbf{w} must be continuous but none of its derivatives need be continuous. For these integrals to exist, sufficient continuity constraints must be placed on the functions and derivatives in the integrands. Since the differentiation is of order 1 in the above formulation then both \mathbf{w} and \mathbf{u} must be at least piecewise linear (so that their derivatives can have only jump discontinuities). The above is called the symmetric weak form of the problem because the highest order of differentiation that appears is the same for both the displacement \mathbf{u} and the weighting function \mathbf{w} . This gives the same constraints on the continuity of both functions and they may both be of class C^0 .

For the two dimensional problem, the weighting function and displacement can be expressed as the column vectors

$$\mathbf{w} = (w_1 \quad w_2)^t \quad (2.14)$$

$$\mathbf{u} = (u_1 \quad u_2)^t \quad (2.15)$$

with the vector transpose operation denoted by a superscript t . Approximate solutions are obtained by utilizing a finite-dimensional representation for these functions. To discretize these fields, values of the displacement and weighting functions

at certain discrete points (these points are nodes in the finite element method) are used with an assumed set of interpolation functions (basis functions) which describe the spatial variation of the field between the points chosen. Mathematically,

$$\mathbf{u} = \mathbf{N}_g \mathbf{u}^n \quad (2.16)$$

$$\mathbf{w} = \mathbf{N}_g \mathbf{w}^n \quad (2.17)$$

where

$$\mathbf{u}^n = (u_1^1 \quad u_2^1 \quad u_1^2 \quad u_2^2 \quad \dots \quad u_1^n \quad u_2^n)^t, \quad (2.18)$$

$$\mathbf{w}^n = (w_1^1 \quad w_2^1 \quad w_1^2 \quad w_2^2 \quad \dots \quad w_1^n \quad w_2^n)^t, \quad (2.19)$$

and \mathbf{N}_g is the matrix of global basis functions

$$\mathbf{N}_g = \begin{pmatrix} N^1 & 0 & N^2 & 0 & \dots & N^n & 0 \\ 0 & N^1 & 0 & N^2 & \dots & 0 & N^n \end{pmatrix}. \quad (2.20)$$

The superscripts denote node numbers and the subscripts denote the rectangular cartesian coordinate directions 1 and 2, i.e. u_1^2 is the displacement in direction 1 at node 2. Note that the basis functions need only be piece-wise linear and can be used for both \mathbf{u} and \mathbf{w} since both are C^0 functions. Using these approximations in Equation (2.13)

$$\int_R (\mathbf{N}_g \mathbf{w}^n \nabla) : \mathbf{C} : (\nabla(\mathbf{N}_g \mathbf{u}^n)) dV = \int_{\partial R_t} \mathbf{N}_g \mathbf{w}^n \cdot \mathbf{t}^* dA \quad (2.21)$$

or, since \mathbf{w}^n is arbitrary and can be factored out,

$$\int_R \mathbf{N}_g \nabla : \mathbf{C} : \nabla(\mathbf{N}_g \mathbf{u}^n) dV = \int_{\partial R_t} \mathbf{N}_g \cdot \mathbf{t}^* dA \quad (2.22)$$

where the term on the left will be separated into the global stiffness matrix \mathbf{K}_g times the vector \mathbf{u}^n (which can be factored out of the integral) and the right side becomes the discretized force vector \mathbf{f} .

To fully discretize the problem, suitable representations of the del differential operator and the elasticity tensor are necessary. The stress and strain tensors are normally expressed as vectors allowing the del operator to be represented as a matrix (\mathbf{L}_g) of differential operators and the elasticity tensor to become a matrix (\mathbf{D}) of elastic parameters. The stiffness matrix can then be described by

$$\mathbf{K}_g = \int_R \mathbf{B}_g^t \mathbf{D} \mathbf{B}_g dR, \quad (2.23)$$

where

$$\mathbf{B}_g = \mathbf{L}_g \mathbf{N}_g. \quad (2.24)$$

The differential operator matrix \mathbf{L}_g for two dimensional elasticity is expressed as

$$\mathbf{L}_g = \begin{pmatrix} \partial_1 & 0 \\ 0 & \partial_2 \\ \frac{\sqrt{2}}{2} \partial_2 & \frac{\sqrt{2}}{2} \partial_1 \end{pmatrix}. \quad (2.25)$$

The operator matrix is defined in this manner in order to express the strain displacement relation as

$$\epsilon = \mathbf{L}_g \mathbf{u}, \quad (2.26)$$

with the strain vector

$$\epsilon = \begin{pmatrix} \epsilon_{11} \\ \epsilon_{22} \\ \sqrt{2} \epsilon_{12} \end{pmatrix}. \quad (2.27)$$

Similarly, the stress tensor is put in vector form as

$$\sigma = \begin{pmatrix} \sigma_{11} \\ \sigma_{22} \\ \sqrt{2} \sigma_{12} \end{pmatrix}, \quad (2.28)$$

and the stress-strain relation becomes

$$\sigma = \mathbf{D} \epsilon, \quad (2.29)$$

where the matrix form of the isotropic elasticity tensor is given by (for the plane strain condition)

$$\mathbf{D} = \frac{E}{(1+\nu)(1-2\nu)} \begin{pmatrix} 1-\nu & \nu & 0 \\ \nu & 1-\nu & 0 \\ 0 & 0 & 1-2\nu \end{pmatrix} \quad (2.30)$$

with E being Young's modulus and ν Poisson's ratio.

Now, to proceed with the two dimensional four node quadrilateral element, the mapping from global coordinates, x_1, x_2 , to local coordinates, r and s , as well as the node numbering scheme is shown in Figure 1. The domain of any element is mapped onto the square whose nodes are located at -1 and 1 in both the local r and s directions. The node numbering begins with 1 at the lower right and proceeds counterclockwise.

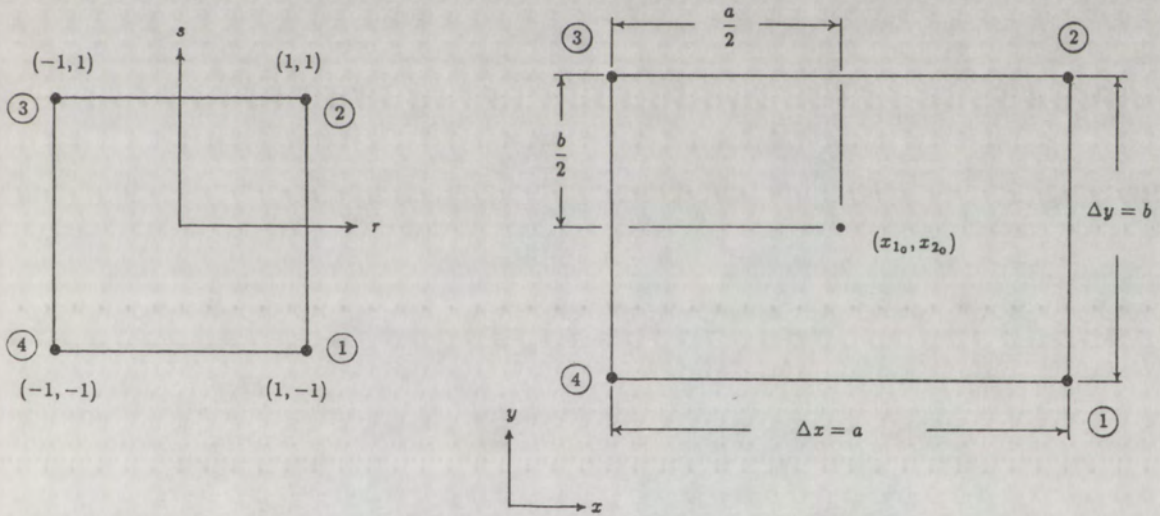


Figure 1. Element Mapping

For the element studied, the standard bilinear shape functions are

$$\begin{aligned} N^1 &= \frac{1}{4}(1+r)(1-s) \\ N^2 &= \frac{1}{4}(1+r)(1+s) \\ N^3 &= \frac{1}{4}(1-r)(1+s) \\ N^4 &= \frac{1}{4}(1-r)(1-s) \end{aligned} \tag{2.31}$$

and the shape function matrix is

$$\mathbf{N} = \begin{pmatrix} N^1 & 0 & N^2 & 0 & N^3 & 0 & N^4 & 0 \\ 0 & N^1 & 0 & N^2 & 0 & N^3 & 0 & N^4 \end{pmatrix}. \quad (2.32)$$

In the global coordinate system the stiffness matrix for the element is given by

$$\mathbf{K} = \int_{x_{10}-\frac{a}{2}}^{x_{10}+\frac{a}{2}} \int_{x_{20}-\frac{b}{2}}^{x_{20}+\frac{b}{2}} \mathbf{B}^t \mathbf{D} \mathbf{B} dx_2 dx_1. \quad (2.33)$$

where x_{10} and x_{20} are the coordinates of the element center, and a and b denote the element dimensions in the x_1 and x_2 directions, respectively. Since the Jacobian of the transformation from global to local coordinates is constant over the domain of the element (note that this holds only for rectangular elements) then the stiffness matrix can be expressed in terms of the local coordinates as

$$\mathbf{K} = \frac{1}{4} ab \int_{-1}^1 \int_{-1}^1 \mathbf{B}^t \mathbf{D} \mathbf{B} dr ds. \quad (2.34)$$

The \mathbf{L}_g matrix is similarly transformed and assumes the following form:

$$\mathbf{L} = \begin{pmatrix} \frac{2}{a} \partial_r & 0 \\ 0 & \frac{2}{b} \partial_s \\ \frac{\sqrt{2}}{b} \partial_s & \frac{\sqrt{2}}{a} \partial_r \end{pmatrix} \quad (2.35)$$

Then, by taking the appropriate derivatives the \mathbf{B} matrix can be determined ($\mathbf{B} = \mathbf{L}\mathbf{N}$), and performing the indicated matrix multiplications, the integrand of Equation (2.34) can be specified in terms of the elastic constants, the element dimensions a and b , and polynomials of the local coordinates r and s . The polynomials are relatively simple (the highest order that appears is quadratic) and are easily integrated either exactly or by any of a number of quadrature rules. The result is an element stiffness matrix whose terms are functions of the elastic constants and the element dimensions. The components of the element stiffness matrix are shown in Figure 2 for an exact integration of Equation (2.34). In this figure, B is the constrained modulus, λ_p is Lamé's parameter, and G is the shear modulus.

$$\begin{array}{ccccccc}
\frac{1}{3} \frac{b}{a} B + \frac{1}{3} \frac{a}{b} G & -\frac{1}{4} \lambda_p - \frac{1}{4} G & \frac{1}{6} \frac{b}{a} B - \frac{1}{3} \frac{a}{b} G & \frac{1}{4} \lambda_p - \frac{1}{4} G & -\frac{1}{6} \frac{b}{a} B - \frac{1}{6} \frac{a}{b} G & \frac{1}{4} \lambda_p + \frac{1}{4} G & -\frac{1}{3} \frac{b}{a} B + \frac{1}{6} \frac{a}{b} G & -\frac{1}{4} \lambda_p + \frac{1}{4} G \\
-\frac{1}{4} \lambda_p - \frac{1}{4} G & \frac{1}{3} \frac{a}{b} B + \frac{1}{3} \frac{b}{a} G & -\frac{1}{4} \lambda_p + \frac{1}{4} G & -\frac{1}{3} \frac{a}{b} B + \frac{1}{6} \frac{b}{a} G & \frac{1}{4} \lambda_p + \frac{1}{4} G & -\frac{1}{6} \frac{a}{b} B - \frac{1}{6} \frac{b}{a} G & \frac{1}{4} \lambda_p - \frac{1}{4} G & \frac{1}{6} \frac{a}{b} B - \frac{1}{3} \frac{b}{a} G \\
\frac{1}{6} \frac{b}{a} B - \frac{1}{3} \frac{a}{b} G & -\frac{1}{4} \lambda_p + \frac{1}{4} G & \frac{1}{3} \frac{a}{b} B + \frac{1}{6} \frac{b}{a} G & \frac{1}{4} \lambda_p + \frac{1}{4} G & -\frac{1}{3} \frac{a}{b} B + \frac{1}{6} \frac{b}{a} G & \frac{1}{4} \lambda_p - \frac{1}{4} G & -\frac{1}{6} \frac{b}{a} B - \frac{1}{6} \frac{a}{b} G & -\frac{1}{4} \lambda_p - \frac{1}{4} G \\
\frac{1}{4} \lambda_p - \frac{1}{4} G & -\frac{1}{3} \frac{a}{b} B + \frac{1}{6} \frac{b}{a} G & \frac{1}{4} \lambda_p + \frac{1}{4} G & \frac{1}{3} \frac{a}{b} B + \frac{1}{6} \frac{b}{a} G & -\frac{1}{4} \lambda_p + \frac{1}{4} G & -\frac{1}{6} \frac{a}{b} B - \frac{1}{6} \frac{b}{a} G & \frac{1}{4} \lambda_p - \frac{1}{4} G & -\frac{1}{3} \frac{a}{b} B - \frac{1}{6} \frac{b}{a} G \\
-\frac{1}{6} \frac{b}{a} B - \frac{1}{3} \frac{a}{b} G & \frac{1}{4} \lambda_p + \frac{1}{4} G & -\frac{1}{3} \frac{a}{b} B + \frac{1}{6} \frac{b}{a} G & -\frac{1}{4} \lambda_p + \frac{1}{4} G & \frac{1}{3} \frac{a}{b} B + \frac{1}{6} \frac{b}{a} G & -\frac{1}{4} \lambda_p - \frac{1}{4} G & \frac{1}{6} \frac{a}{b} B - \frac{1}{3} \frac{b}{a} G & \frac{1}{4} \lambda_p - \frac{1}{4} G \\
\frac{1}{4} \lambda_p + \frac{1}{4} G & -\frac{1}{6} \frac{a}{b} B - \frac{1}{6} \frac{b}{a} G & \frac{1}{4} \lambda_p - \frac{1}{4} G & \frac{1}{3} \frac{a}{b} B - \frac{1}{6} \frac{b}{a} G & -\frac{1}{4} \lambda_p - \frac{1}{4} G & -\frac{1}{6} \frac{a}{b} B + \frac{1}{6} \frac{b}{a} G & \frac{1}{4} \lambda_p + \frac{1}{4} G & -\frac{1}{3} \frac{a}{b} B + \frac{1}{6} \frac{b}{a} G \\
-\frac{1}{3} \frac{a}{b} B + \frac{1}{6} \frac{b}{a} G & \frac{1}{4} \lambda_p - \frac{1}{4} G & -\frac{1}{6} \frac{a}{b} B - \frac{1}{6} \frac{b}{a} G & -\frac{1}{4} \lambda_p - \frac{1}{4} G & \frac{1}{3} \frac{a}{b} B - \frac{1}{6} \frac{b}{a} G & \frac{1}{4} \lambda_p + \frac{1}{4} G & \frac{1}{6} \frac{a}{b} B + \frac{1}{3} \frac{b}{a} G & \frac{1}{4} \lambda_p + \frac{1}{4} G \\
-\frac{1}{4} \lambda_p + \frac{1}{4} G & \frac{1}{6} \frac{a}{b} B - \frac{1}{6} \frac{b}{a} G & -\frac{1}{4} \lambda_p - \frac{1}{4} G & -\frac{1}{3} \frac{a}{b} B + \frac{1}{6} \frac{b}{a} G & \frac{1}{4} \lambda_p - \frac{1}{4} G & -\frac{1}{6} \frac{a}{b} B + \frac{1}{6} \frac{b}{a} G & \frac{1}{4} \lambda_p + \frac{1}{4} G & \frac{1}{3} \frac{a}{b} B + \frac{1}{6} \frac{b}{a} G
\end{array}$$

$$B = \frac{E(1-\nu)}{(1+\nu)(1-2\nu)}$$

$$\lambda_p = \frac{E\nu}{(1+\nu)(1-2\nu)}$$

$$G = \frac{E}{2(1+\nu)}$$

Figure 2. Components of Fully Integrated Element Stiffness Matrix

II.B. Numerical Integration

Many finite element codes evaluate the integrals that define the stiffness matrices (and others, like the mass matrix in dynamic codes) by Gaussian quadrature. This method of numerical integration yields the exact value of the integral for polynomial integrands if a sufficient number of quadrature points is used. The relationship between the order of the polynomial, n , and the number of quadrature points, m , required to evaluate the integral exactly is

$$n \leq 2m - 1 \quad (2.36)$$

Thus to exactly integrate the quadratic polynomials that occur (in both the r and the s directions) in the integrand of the stiffness matrix, at least two quadrature points are needed in both (r and s) directions. This results in a total of four quadrature points to have the numerical integration yield the same value as a closed form solution (within round-off error). The most commonly used underintegration is the use of only one quadrature point. Others that are used less often are (2×1) and (1×2) which denote two quadrature points in the r direction and only 1 in s , and vice-versa, respectively. These schemes give a full integration in one direction and an underintegration in the other. The resulting element stiffness matrices for these other integrations are shown in Figures 3 through 5 for a (2×1) , a (1×2) , and a (1×1) integration, respectively.

$$\begin{array}{cccccccc}
\frac{1}{4} \frac{b}{a} B + \frac{1}{3} \frac{a}{b} G & -\frac{1}{4} \lambda_p - \frac{1}{4} G & \frac{1}{4} \frac{b}{a} B - \frac{1}{3} \frac{a}{b} G & \frac{1}{4} \lambda_p - \frac{1}{4} G & -\frac{1}{4} \frac{b}{a} B - \frac{1}{6} \frac{a}{b} G & \frac{1}{4} \lambda_p + \frac{1}{4} G & -\frac{1}{4} \frac{b}{a} B + \frac{1}{6} \frac{a}{b} G & -\frac{1}{4} \lambda_p + \frac{1}{4} G \\
-\frac{1}{4} \lambda_p - \frac{1}{4} G & \frac{1}{3} \frac{a}{b} B + \frac{1}{4} \frac{b}{a} G & -\frac{1}{4} \lambda_p + \frac{1}{4} G & -\frac{1}{3} \frac{a}{b} B + \frac{1}{4} \frac{b}{a} G & -\frac{1}{4} \lambda_p + \frac{1}{4} G & -\frac{1}{6} \frac{a}{b} B - \frac{1}{4} \frac{b}{a} G & \frac{1}{4} \lambda_p - \frac{1}{4} G & \frac{1}{6} \frac{a}{b} B - \frac{1}{4} \frac{b}{a} G \\
\frac{1}{4} \frac{b}{a} B - \frac{1}{3} \frac{a}{b} G & -\frac{1}{4} \lambda_p + \frac{1}{4} G & \frac{1}{4} \frac{b}{a} B + \frac{1}{3} \frac{a}{b} G & \frac{1}{4} \lambda_p + \frac{1}{4} G & -\frac{1}{4} \frac{b}{a} B + \frac{1}{6} \frac{a}{b} G & \frac{1}{4} \lambda_p - \frac{1}{4} G & -\frac{1}{4} \frac{b}{a} B - \frac{1}{6} \frac{a}{b} G & -\frac{1}{4} \lambda_p - \frac{1}{4} G \\
\frac{1}{4} \lambda_p - \frac{1}{4} G & -\frac{1}{3} \frac{a}{b} B + \frac{1}{4} \frac{b}{a} G & \frac{1}{4} \lambda_p + \frac{1}{4} G & \frac{1}{3} \frac{a}{b} B + \frac{1}{4} \frac{b}{a} G & -\frac{1}{4} \lambda_p + \frac{1}{4} G & \frac{1}{6} \frac{a}{b} B - \frac{1}{4} \frac{b}{a} G & -\frac{1}{4} \lambda_p - \frac{1}{4} G & -\frac{1}{6} \frac{a}{b} B - \frac{1}{4} \frac{b}{a} G \\
-\frac{1}{4} \frac{b}{a} B - \frac{1}{6} \frac{a}{b} G & \frac{1}{4} \lambda_p + \frac{1}{4} G & -\frac{1}{4} \frac{b}{a} B + \frac{1}{3} \frac{a}{b} G & -\frac{1}{4} \lambda_p + \frac{1}{4} G & \frac{1}{4} \frac{b}{a} B + \frac{1}{6} \frac{a}{b} G & -\frac{1}{4} \lambda_p - \frac{1}{4} G & \frac{1}{4} \frac{b}{a} B - \frac{1}{6} \frac{a}{b} G & \frac{1}{4} \lambda_p - \frac{1}{4} G \\
\frac{1}{4} \lambda_p + \frac{1}{4} G & -\frac{1}{6} \frac{a}{b} B - \frac{1}{4} \frac{b}{a} G & \frac{1}{4} \lambda_p - \frac{1}{4} G & \frac{1}{6} \frac{a}{b} B - \frac{1}{4} \frac{b}{a} G & -\frac{1}{4} \lambda_p - \frac{1}{4} G & \frac{1}{3} \frac{a}{b} B + \frac{1}{4} \frac{b}{a} G & -\frac{1}{4} \lambda_p + \frac{1}{4} G & -\frac{1}{3} \frac{a}{b} B + \frac{1}{4} \frac{b}{a} G \\
-\frac{1}{4} \lambda_p + \frac{1}{4} G & \frac{1}{6} \frac{a}{b} B - \frac{1}{4} \frac{b}{a} G & -\frac{1}{4} \frac{b}{a} B - \frac{1}{3} \frac{a}{b} G & -\frac{1}{4} \lambda_p - \frac{1}{4} G & \frac{1}{4} \frac{b}{a} B - \frac{1}{6} \frac{a}{b} G & -\frac{1}{4} \lambda_p + \frac{1}{4} G & \frac{1}{4} \frac{b}{a} B + \frac{1}{6} \frac{a}{b} G & \frac{1}{4} \lambda_p + \frac{1}{4} G \\
-\frac{1}{4} \lambda_p + \frac{1}{4} G & \frac{1}{6} \frac{a}{b} B - \frac{1}{4} \frac{b}{a} G & -\frac{1}{4} \lambda_p - \frac{1}{4} G & -\frac{1}{6} \frac{a}{b} B - \frac{1}{4} \frac{b}{a} G & -\frac{1}{4} \lambda_p - \frac{1}{4} G & -\frac{1}{3} \frac{a}{b} B + \frac{1}{4} \frac{b}{a} G & \frac{1}{4} \lambda_p + \frac{1}{4} G & \frac{1}{3} \frac{a}{b} B + \frac{1}{4} \frac{b}{a} G
\end{array}$$

$$B = \frac{E(1-\nu)}{(1+\nu)(1-2\nu)}$$

$$\lambda_p = \frac{E\nu}{(1+\nu)(1-2\nu)}$$

$$G = \frac{E}{2(1+\nu)}$$

Figure 3. Components of a 2×1 Integration of the Element Stiffness Matrix

$$\begin{array}{cccccccc}
\frac{1}{3} \frac{b}{a} B + \frac{1}{4} \frac{a}{b} G & -\frac{1}{4} \lambda_p - \frac{1}{4} G & \frac{1}{6} \frac{b}{a} B - \frac{1}{4} \frac{a}{b} G & \frac{1}{4} \lambda_p - \frac{1}{4} G & -\frac{1}{6} \frac{b}{a} B - \frac{1}{4} \frac{a}{b} G & \frac{1}{4} \lambda_p + \frac{1}{4} G & -\frac{1}{3} \frac{b}{a} B + \frac{1}{4} \frac{a}{b} G & -\frac{1}{4} \lambda_p + \frac{1}{4} G \\
-\frac{1}{4} \lambda_p - \frac{1}{4} G & \frac{1}{4} \frac{a}{b} B + \frac{1}{3} \frac{b}{a} G & -\frac{1}{4} \lambda_p + \frac{1}{4} G & -\frac{1}{4} \frac{a}{b} B + \frac{1}{6} \frac{b}{a} G & -\frac{1}{4} \lambda_p + \frac{1}{4} G & -\frac{1}{4} \frac{a}{b} B - \frac{1}{6} \frac{b}{a} G & \frac{1}{4} \lambda_p - \frac{1}{4} G & \frac{1}{4} \frac{a}{b} B - \frac{1}{3} \frac{b}{a} G \\
\frac{1}{6} \frac{b}{a} B - \frac{1}{4} \frac{a}{b} G & -\frac{1}{4} \lambda_p + \frac{1}{4} G & \frac{1}{3} \frac{b}{a} B + \frac{1}{4} \frac{a}{b} G & \frac{1}{4} \lambda_p + \frac{1}{4} G & -\frac{1}{3} \frac{b}{a} B + \frac{1}{4} \frac{a}{b} G & \frac{1}{4} \lambda_p - \frac{1}{4} G & -\frac{1}{6} \frac{b}{a} B - \frac{1}{4} \frac{a}{b} G & -\frac{1}{4} \lambda_p - \frac{1}{4} G \\
\frac{1}{4} \lambda_p - \frac{1}{4} G & -\frac{1}{4} \frac{a}{b} B + \frac{1}{6} \frac{b}{a} G & \frac{1}{4} \lambda_p + \frac{1}{4} G & \frac{1}{4} \frac{a}{b} B + \frac{1}{3} \frac{b}{a} G & -\frac{1}{4} \lambda_p + \frac{1}{4} G & \frac{1}{4} \frac{a}{b} B - \frac{1}{6} \frac{b}{a} G & -\frac{1}{4} \lambda_p - \frac{1}{4} G & -\frac{1}{4} \frac{a}{b} B - \frac{1}{6} \frac{b}{a} G \\
-\frac{1}{6} \frac{b}{a} B - \frac{1}{4} \frac{a}{b} G & \frac{1}{4} \lambda_p + \frac{1}{4} G & -\frac{1}{6} \frac{b}{a} B + \frac{1}{4} \frac{a}{b} G & -\frac{1}{4} \lambda_p + \frac{1}{4} G & \frac{1}{3} \frac{b}{a} B + \frac{1}{4} \frac{a}{b} G & -\frac{1}{4} \lambda_p - \frac{1}{4} G & \frac{1}{6} \frac{b}{a} B - \frac{1}{4} \frac{a}{b} G & \frac{1}{4} \lambda_p - \frac{1}{4} G \\
\frac{1}{4} \lambda_p + \frac{1}{4} G & -\frac{1}{4} \frac{a}{b} B - \frac{1}{6} \frac{b}{a} G & \frac{1}{4} \lambda_p - \frac{1}{4} G & \frac{1}{4} \frac{a}{b} B - \frac{1}{3} \frac{b}{a} G & -\frac{1}{4} \lambda_p - \frac{1}{4} G & \frac{1}{4} \frac{a}{b} B + \frac{1}{6} \frac{b}{a} G & -\frac{1}{4} \lambda_p + \frac{1}{4} G & -\frac{1}{4} \frac{a}{b} B + \frac{1}{6} \frac{b}{a} G \\
-\frac{1}{3} \frac{b}{a} B + \frac{1}{4} \frac{a}{b} G & \frac{1}{4} \lambda_p - \frac{1}{4} G & -\frac{1}{6} \frac{b}{a} B - \frac{1}{4} \frac{a}{b} G & -\frac{1}{4} \lambda_p - \frac{1}{4} G & \frac{1}{6} \frac{b}{a} B - \frac{1}{4} \frac{a}{b} G & \frac{1}{3} \frac{b}{a} B + \frac{1}{4} \frac{a}{b} G & \frac{1}{4} \lambda_p + \frac{1}{4} G & \frac{1}{4} \lambda_p + \frac{1}{4} G \\
-\frac{1}{4} \lambda_p + \frac{1}{4} G & \frac{1}{4} \frac{a}{b} B - \frac{1}{3} \frac{b}{a} G & -\frac{1}{4} \lambda_p - \frac{1}{4} G & -\frac{1}{4} \frac{a}{b} B - \frac{1}{6} \frac{b}{a} G & -\frac{1}{4} \lambda_p - \frac{1}{4} G & -\frac{1}{4} \frac{a}{b} B + \frac{1}{6} \frac{b}{a} G & \frac{1}{4} \lambda_p + \frac{1}{4} G & \frac{1}{4} \frac{a}{b} B + \frac{1}{3} \frac{b}{a} G
\end{array}$$

$$B = \frac{E(1-\nu)}{(1+\nu)(1-2\nu)}$$

$$\lambda_p = \frac{E\nu}{(1+\nu)(1-2\nu)}$$

$$G = \frac{E}{2(1+\nu)}$$

Figure 4. Components of a 1x2 Integration of the Element Stiffness Matrix

$$\begin{array}{cccccccc}
\frac{1}{4} \frac{b}{a} B + \frac{1}{4} \frac{a}{b} G & -\frac{1}{4} \lambda_p - \frac{1}{4} G & \frac{1}{4} \frac{b}{a} B - \frac{1}{4} \frac{a}{b} G & \frac{1}{4} \lambda_p - \frac{1}{4} G & -\frac{1}{4} \frac{b}{a} B - \frac{1}{4} \frac{a}{b} G & \frac{1}{4} \lambda_p + \frac{1}{4} G & -\frac{1}{4} \frac{b}{a} B + \frac{1}{4} \frac{a}{b} G & -\frac{1}{4} \lambda_p + \frac{1}{4} G \\
-\frac{1}{4} \lambda_p - \frac{1}{4} G & \frac{1}{4} \frac{a}{b} B + \frac{1}{4} \frac{b}{a} G & -\frac{1}{4} \lambda_p + \frac{1}{4} G & -\frac{1}{4} \frac{a}{b} B + \frac{1}{4} \frac{b}{a} G & -\frac{1}{4} \frac{a}{b} B + \frac{1}{4} \frac{b}{a} G & \frac{1}{4} \lambda_p + \frac{1}{4} G & -\frac{1}{4} \frac{a}{b} B - \frac{1}{4} \frac{b}{a} G & \frac{1}{4} \frac{a}{b} B - \frac{1}{4} \frac{b}{a} G \\
\frac{1}{4} \frac{b}{a} B - \frac{1}{4} \frac{a}{b} G & -\frac{1}{4} \lambda_p + \frac{1}{4} G & \frac{1}{4} \frac{b}{a} B + \frac{1}{4} \frac{a}{b} G & \frac{1}{4} \lambda_p + \frac{1}{4} G & -\frac{1}{4} \frac{b}{a} B + \frac{1}{4} \frac{a}{b} G & \frac{1}{4} \lambda_p - \frac{1}{4} G & -\frac{1}{4} \frac{b}{a} B - \frac{1}{4} \frac{a}{b} G & -\frac{1}{4} \lambda_p - \frac{1}{4} G \\
\frac{1}{4} \lambda_p - \frac{1}{4} G & -\frac{1}{4} \frac{a}{b} B + \frac{1}{4} \frac{b}{a} G & \frac{1}{4} \lambda_p + \frac{1}{4} G & \frac{1}{4} \frac{a}{b} B + \frac{1}{4} \frac{b}{a} G & -\frac{1}{4} \lambda_p + \frac{1}{4} G & \frac{1}{4} \frac{a}{b} B - \frac{1}{4} \frac{b}{a} G & -\frac{1}{4} \lambda_p - \frac{1}{4} G & -\frac{1}{4} \frac{a}{b} B - \frac{1}{4} \frac{b}{a} G \\
-\frac{1}{4} \frac{b}{a} B - \frac{1}{4} \frac{a}{b} G & \frac{1}{4} \lambda_p + \frac{1}{4} G & -\frac{1}{4} \frac{b}{a} B + \frac{1}{4} \frac{a}{b} G & -\frac{1}{4} \lambda_p + \frac{1}{4} G & \frac{1}{4} \frac{b}{a} B - \frac{1}{4} \frac{a}{b} G & -\frac{1}{4} \lambda_p - \frac{1}{4} G & \frac{1}{4} \frac{b}{a} B - \frac{1}{4} \frac{a}{b} G & \frac{1}{4} \lambda_p - \frac{1}{4} G \\
\frac{1}{4} \lambda_p + \frac{1}{4} G & -\frac{1}{4} \frac{a}{b} B - \frac{1}{4} \frac{b}{a} G & \frac{1}{4} \lambda_p - \frac{1}{4} G & \frac{1}{4} \frac{a}{b} B - \frac{1}{4} \frac{b}{a} G & -\frac{1}{4} \lambda_p - \frac{1}{4} G & \frac{1}{4} \frac{a}{b} B + \frac{1}{4} \frac{b}{a} G & -\frac{1}{4} \lambda_p + \frac{1}{4} G & -\frac{1}{4} \frac{a}{b} B + \frac{1}{4} \frac{b}{a} G \\
-\frac{1}{4} \frac{b}{a} B + \frac{1}{4} \frac{a}{b} G & \frac{1}{4} \lambda_p - \frac{1}{4} G & -\frac{1}{4} \frac{b}{a} B - \frac{1}{4} \frac{a}{b} G & -\frac{1}{4} \lambda_p - \frac{1}{4} G & \frac{1}{4} \frac{b}{a} B - \frac{1}{4} \frac{a}{b} G & -\frac{1}{4} \lambda_p + \frac{1}{4} G & \frac{1}{4} \frac{b}{a} B + \frac{1}{4} \frac{a}{b} G & \frac{1}{4} \lambda_p + \frac{1}{4} G \\
-\frac{1}{4} \lambda_p + \frac{1}{4} G & \frac{1}{4} \frac{a}{b} B - \frac{1}{4} \frac{b}{a} G & -\frac{1}{4} \lambda_p - \frac{1}{4} G & -\frac{1}{4} \frac{a}{b} B + \frac{1}{4} \frac{b}{a} G & -\frac{1}{4} \lambda_p - \frac{1}{4} G & -\frac{1}{4} \frac{a}{b} B + \frac{1}{4} \frac{b}{a} G & \frac{1}{4} \lambda_p + \frac{1}{4} G & \frac{1}{4} \frac{a}{b} B + \frac{1}{4} \frac{b}{a} G
\end{array}$$

14

$$B = \frac{E(1-\nu)}{(1+\nu)(1-2\nu)}$$

$$\lambda_p = \frac{E\nu}{(1+\nu)(1-2\nu)}$$

$$G = \frac{E}{2(1+\nu)}$$

Figure 5. Components of One-Point Integration of the Element Stiffness Matrix

II.C. Detailed Description of the Problem

Finite element solutions, in general, converge to the exact solution of a problem as the elements that make up the mesh become smaller and smaller. As the mesh becomes more and more refined, the number of elements and nodes used to model the problem increases. The region over which the assumptions made about the variation of the field variables (basis functions) become smaller and therefore less constraining. Thus, as the mesh is refined, the discretized approximation (finite element representation) approaches the actual continuous nature of the problem. But it is usually too costly (in terms of computer time) to use such small elements and a compromise is made. The element size is chosen such that the computer run time is acceptable, knowing that the solution will be slightly stiffer than the exact solution.

The stiffness exhibited by some elements in certain situations greatly exceeds the stiffness that would normally be associated with a given mesh. In particular, the four node quadrilateral is excessively stiff in its response to the simple bending of a beam. This behavior remains even for very refined meshes. Errors of this nature (that do not disappear with mesh refinement) are termed in the literature as errors of the second kind (Prathap, 1985), while those that are removed by a smaller mesh are called errors of the first kind.

It has commonly been held that errors of the second kind were due to an element aspect ratio (the ratio between the two element dimensions, generally length a to width b) that was larger than one. The error has been seen to increase as the aspect ratio increases. Since the element was developed with the standard shape of a square but is often used in other shapes, MacNeal and Harder (1985) recommend that the four node quadrilateral element be tested for large aspect ratios (and other common non-standard shapes). Thus the behavior of the element is studied here for large aspect ratios.

Prathap (1985) contends, however, that it is not the element aspect ratio that causes these errors of the second kind in the plane stress modelling of cantilever beams. Instead, it is the ratio of the element length, in this case a , to the beam thickness, d , that dominates the result. He has defined an additional stiffness parameter, e , based on this ratio and Poisson's ratio as follows:

$$e_1 = \frac{1}{1 - \nu^2} + \frac{Ga^2}{Ed^2} - 1 \quad (2.37)$$

$$e_\infty = \frac{Ga^2}{Ed^2} \quad (2.38)$$

$$e_{fem} = \frac{w(theory)}{w(fem)} - 1 \quad (2.39)$$

Here e_1 is used to predict the additional stiffness parameter when only one element is used through the thickness of the beam, e_∞ when many elements are used, and e_{fem} to compare the finite element results with the predictions. The transverse displacement at the neutral axis is denoted by w . Again, in this formulation it is not the aspect ratio but the ratio of element length to beam thickness that governs the excess stiffness of the finite element approximation of the beam response. This interpretation will also be investigated.

Variations in material properties can also greatly affect the response of the element. In this case the problem occurs when the material is said to become incompressible (Poisson's ratio, ν , approaches 0.5). The term incompressible is used because the volumetric (or bulk) stiffness of the material becomes very large in comparison with its shear stiffness. This can be seen in the elasticity matrix \mathbf{D} defined by Equation (2.30). As ν approaches 0.5, the quantity $(1 - 2\nu)$ in the denominator approaches zero and the volumetric terms in the matrix become large.

The shear term, however, varies only from E to $E/1.5$ as ν goes from 0 to 0.5 and thus remains relatively unchanged. For bending problems in which shear terms play an important part, the element is dominated by the volumetric terms and yields overly stiff results for nearly incompressible materials. Zienkiewicz (1977) separated the volumetric from the shear terms by expressing \mathbf{D} in the form

$$\mathbf{D} = \mathbf{D}_1 + \mathbf{D}_2 \quad (2.40)$$

$$\mathbf{D}_1 = G \begin{pmatrix} 2 & 0 & 0 \\ 0 & 2 & 0 \\ 0 & 0 & 2 \end{pmatrix} \quad (2.41)$$

$$\mathbf{D}_2 = \left(K - \frac{2}{3}G\right) \begin{pmatrix} 1 & 1 & 0 \\ 1 & 1 & 0 \\ 0 & 0 & 0 \end{pmatrix} \quad (2.42)$$

where the bulk modulus, K , is

$$K = \frac{E}{3(1 - 2\nu)}. \quad (2.43)$$

If the element stiffness matrix is decomposed into the sum

$$\mathbf{K} = \mathbf{K}_1 + \mathbf{K}_2 \quad (2.44)$$

where

$$\mathbf{K}_1 = \frac{1}{4}ab \int_{-1}^1 \int_{-1}^1 \mathbf{B}^t \mathbf{D}_1 \mathbf{B} dr ds \quad (2.45)$$

$$\mathbf{K}_2 = \frac{1}{4}ab \int_{-1}^1 \int_{-1}^1 \mathbf{B}^t \mathbf{D}_2 \mathbf{B} dr ds \quad (2.46)$$

then the large volumetric terms are isolated in the stiffness matrix \mathbf{K}_2 . A one-point integration is then applied to evaluate \mathbf{K}_2 which relaxes the volumetric stiffness (in bending). The matrix \mathbf{K}_1 is fully integrated and therefore is of sufficient rank

that the overall system is not singular due to the singularity of \mathbf{K}_2 caused by underintegration. Because the reduced integration is selectively applied to \mathbf{K}_2 , the procedure is called selective-reduced or reduced-selective integration. The element stiffness matrix that results from this kind of integration is given in Figure 6.

Even though reduced-selective integration gives reasonably good results, it is not used very much with this element. The main reason for this is that it requires more effort to keep track of the two parts of the stiffness matrix (more computer time and memory). A four point integration is applied to evaluate the components of one matrix (costly in itself), and then yet another matrix of the same size must be determined. This process is more costly than even a full integration of Equation (2.34) because there are two stiffness matrices to keep separate and operate on.

A one-point integration in Equation (2.34) is much more efficient for evaluating the element stiffness matrix than either of the methods discussed above. The number of operations required is decreased by at least a factor of four (one point as opposed to four points) when compared to a full integration. For dynamic problems solved with explicit time integration, a similar reduction in computations is noted.

But the one-point integration, while efficient, can lead to problems. For certain loading and boundary conditions, a one-point integration can lead to singularities in static solutions (which disallow inversion of the stiffness matrix) or instabilities in dynamic solutions called hourglassing. The term hourglassing is used because the nodes in the mesh oscillate causing adjoining elements to make a shape that looks like an hourglass. In problems that require the element to bend (as in the beam flexure problem), the hourglassing can increase to the point that it dominates or obscures the actual solution. Methods of hourglass control must then be used, some of which can distort the solution themselves. Therefore, the initial appeal of one-point integration can quickly wear off if one is not prepared to address the problems of hourglassing and singularities.

$C_{1\frac{b}{a}} + \frac{1}{3}\frac{a}{b}G$	$-\frac{1}{4}\lambda_p - \frac{1}{4}G$	$C_{2\frac{b}{a}} - \frac{1}{3}\frac{a}{b}G$	$\frac{1}{4}\lambda_p - \frac{1}{4}G$	$-C_{2\frac{b}{a}} - \frac{1}{6}\frac{a}{b}G$	$\frac{1}{4}\lambda_p + \frac{1}{4}G$	$-C_{1\frac{b}{a}} + \frac{1}{6}\frac{a}{b}G$	$-\frac{1}{4}\lambda_p + \frac{1}{4}G$
$-\frac{1}{4}\lambda_p - \frac{1}{4}G$	$C_{1\frac{a}{b}} + \frac{1}{3}\frac{b}{a}G$	$-\frac{1}{4}\lambda_p + \frac{1}{4}G$	$-C_{1\frac{a}{b}} + \frac{1}{6}\frac{b}{a}G$	$\frac{1}{4}\lambda_p + \frac{1}{4}G$	$-C_{2\frac{a}{b}} - \frac{1}{6}\frac{b}{a}G$	$\frac{1}{4}\lambda_p - \frac{1}{4}G$	$C_{2\frac{a}{b}} - \frac{1}{3}\frac{b}{a}G$
$C_{2\frac{b}{a}} - \frac{1}{3}\frac{a}{b}G$	$-\frac{1}{4}\lambda_p + \frac{1}{4}G$	$C_{1\frac{b}{a}} + \frac{1}{3}\frac{a}{b}G$	$\frac{1}{4}\lambda_p + \frac{1}{4}G$	$-C_{1\frac{b}{a}} + \frac{1}{6}\frac{a}{b}G$	$\frac{1}{4}\lambda_p - \frac{1}{4}G$	$-C_{2\frac{b}{a}} - \frac{1}{6}\frac{a}{b}G$	$-\frac{1}{4}\lambda_p - \frac{1}{4}G$
$\frac{1}{4}\lambda_p - \frac{1}{4}G$	$-C_{1\frac{a}{b}} + \frac{1}{6}\frac{b}{a}G$	$\frac{1}{4}\lambda_p + \frac{1}{4}G$	$C_{1\frac{a}{b}} + \frac{1}{3}\frac{b}{a}G$	$-\frac{1}{4}\lambda_p + \frac{1}{4}G$	$C_{2\frac{a}{b}} - \frac{1}{6}\frac{b}{a}G$	$-\frac{1}{4}\lambda_p - \frac{1}{4}G$	$-C_{2\frac{a}{b}} - \frac{1}{6}\frac{b}{a}G$
$-C_{2\frac{b}{a}} - \frac{1}{6}\frac{a}{b}G$	$\frac{1}{4}\lambda_p + \frac{1}{4}G$	$-C_{1\frac{b}{a}} + \frac{1}{6}\frac{a}{b}G$	$-\frac{1}{4}\lambda_p + \frac{1}{4}G$	$C_{1\frac{b}{a}} + \frac{1}{3}\frac{a}{b}G$	$-\frac{1}{4}\lambda_p - \frac{1}{4}G$	$C_{2\frac{b}{a}}B - \frac{1}{3}\frac{a}{b}G$	$\frac{1}{4}\lambda_p - \frac{1}{4}G$
$\frac{1}{4}\lambda_p + \frac{1}{4}G$	$-C_{2\frac{a}{b}} - \frac{1}{6}\frac{b}{a}G$	$\frac{1}{4}\lambda_p - \frac{1}{4}G$	$C_{2\frac{a}{b}} - \frac{1}{3}\frac{b}{a}G$	$-\frac{1}{4}\lambda_p - \frac{1}{4}G$	$C_{1\frac{a}{b}} + \frac{1}{3}\frac{b}{a}G$	$-\frac{1}{4}\lambda_p + \frac{1}{4}G$	$-C_{1\frac{a}{b}}B + \frac{1}{6}\frac{b}{a}G$
$-C_{1\frac{b}{a}} + \frac{1}{6}\frac{a}{b}G$	$\frac{1}{4}\lambda_p - \frac{1}{4}G$	$-C_{2\frac{b}{a}} - \frac{1}{6}\frac{a}{b}G$	$-\frac{1}{4}\lambda_p - \frac{1}{4}G$	$C_{2\frac{b}{a}} - \frac{1}{6}\frac{a}{b}G$	$-\frac{1}{4}\lambda_p - \frac{1}{4}G$	$C_{1\frac{b}{a}} + \frac{1}{3}\frac{a}{b}G$	$\frac{1}{4}\lambda_p + \frac{1}{4}G$
$-\frac{1}{4}\lambda_p + \frac{1}{4}G$	$C_{2\frac{a}{b}} - \frac{1}{3}\frac{b}{a}G$	$-\frac{1}{4}\lambda_p - \frac{1}{4}G$	$C_{2\frac{a}{b}} - \frac{1}{6}\frac{b}{a}G$	$-\frac{1}{4}\lambda_p - \frac{1}{4}G$	$-C_{1\frac{a}{b}} - \frac{1}{6}\frac{b}{a}G$	$\frac{1}{4}\lambda_p + \frac{1}{4}G$	$C_{1\frac{a}{b}} + \frac{1}{3}\frac{b}{a}G$

19

$$B = \frac{E(1-\nu)}{(1+\nu)(1-2\nu)} \quad \lambda_p = \frac{E\nu}{(1+\nu)(1-2\nu)} \quad G = \frac{E}{2(1+\nu)}$$

$$C_1 = \frac{1}{3}B - \frac{1}{12}\lambda_p \quad C_2 = \frac{1}{6}B + \frac{1}{12}\lambda_p$$

Figure 6. Components of Element Stiffness Matrix Evaluated by Reduced-Selective Integration

So far, this study has shown the differences in the element stiffness matrix for the various integration schemes that produce "less stiff" results. But to clearly see what these differences mean to the response of an element, it is instructive to examine the eigenvalues and eigenvectors of the element and their variations with integration as well as aspect ratio and material properties. While the eigenproblem has been solved for this element under certain conditions (given aspect ratio, material properties, and integration), the explicit analytical expressions for the eigenpairs presented in the next section have not as yet appeared in the literature.

III. Eigenvalue-Eigenvector Interpretation of the Problem

The standard eigenproblem can be stated as follows: if a vector \mathbf{v} can be found such that \mathbf{A} maps \mathbf{v} into a scalar λ times \mathbf{v} , then λ is called an eigenvalue and \mathbf{v} an eigenvector. Normally there are several solutions:

$$(\mathbf{A} - \lambda_{(i)}\mathbf{I})\mathbf{v}_{(i)} = \mathbf{0} \quad (3.1)$$

where λ_i are the eigenvalues, and \mathbf{v}_i are the corresponding eigenvectors of the matrix \mathbf{A} . The matrix \mathbf{I} is the identity matrix which is composed of 1's along the diagonal and 0's everywhere else. The parenthesized indices indicate that there is no summation on i , which will range from 1 to the order of \mathbf{A} .

When the element stiffness matrix \mathbf{K} is substituted for \mathbf{A} in Equation (3.1) the result will be eight eigenvalue-eigenvector pairs which are measures of the response of the element. The eigenvalues indicate the stiffness of the element in its resistance to deformation into the shape of the corresponding eigenvector. Thus, for an increasing eigenvalue, it is more and more difficult to deform the element into the given mode (eigenvector). Conversely, if an eigenvalue is very small or zero, then it takes little or no energy to excite that mode. Note that the rigid body modes should have zero eigenvalues. The hourglass modes show up as additional modes with zero eigenvalues and occur when a one-point integration is used.

Since the stiffness matrix for the four node quadrilateral has been derived in terms of the material properties and element dimensions, then the eigenpairs can also be determined as functions of these parameters. The method by which the functional relationships were found is as follows. Mode shapes for a square element were found in Bathe (1982) for a given value of E and ν . The eigenvectors were then hypothesized from these shapes and used with the stiffness matrix to solve for the corresponding eigenvalues. The most straightforward shapes were checked out first to provide orthogonality comparisons with the other shapes. For the square element

the eigenvectors were composed of constants and the eigenvalues were functions of the elastic quantities.

To extend these findings to elements with aspect ratios other than one a proportionality constant k was included in every other component of the eigenvector. Again, the postulated eigenvectors were used to solve for the unknown eigenvalues and constants k . Due to the symmetries of the element (and thus in the stiffness matrix), certain terms cancelled out in the course of the matrix multiplications yielding (at the worst) quadratic equations for k and a unique solution to the problem. The following equations provide a summary of the eigenpairs obtained for the fully integrated stiffness matrix:

Rigid Body Mode (r direction):

$$\begin{aligned}\lambda_1 &= 0 \\ \mathbf{v}_1 &= (1 \ 0 \ 1 \ 0 \ 1 \ 0 \ 1 \ 0)^t\end{aligned}\tag{3.3}$$

Rigid Body Mode (s direction):

$$\begin{aligned}\lambda_2 &= 0 \\ \mathbf{v}_2 &= (0 \ 1 \ 0 \ 1 \ 0 \ 1 \ 0 \ 1)^t\end{aligned}\tag{3.4}$$

Rigid Body Mode (rotation):

$$\begin{aligned}\lambda_3 &= 0 \\ \mathbf{v}_3 &= (0 \ 0 \ -b\theta \ 0 \ -b\theta \ -a\theta \ 0 \ -a\theta)^t \\ \theta &= \frac{1}{\sqrt{(a^2 + b^2)}}\end{aligned}\tag{3.5}$$

Flexure Mode 1:

$$\begin{aligned}\lambda_4 &= \frac{1}{3}\left(\frac{b}{a}B + \frac{a}{b}G\right) \\ \mathbf{v}_4 &= (1 \ 0 \ -1 \ 0 \ 1 \ 0 \ -1 \ 0)^t\end{aligned}\tag{3.6}$$

Flexure Mode 2:

$$\begin{aligned}\lambda_5 &= \frac{1}{3} \left(\frac{a}{b} B + \frac{b}{a} G \right) \\ \mathbf{v}_5 &= (0 \quad 1 \quad 0 \quad -1 \quad 0 \quad 1 \quad 0 \quad -1)^t\end{aligned}\tag{3.7}$$

Shear Mode:

$$\begin{aligned}\lambda_6 &= G \left(\frac{b}{a} + \frac{a}{b} \right) \\ \mathbf{v}_6 &= (1 \quad -k_6 \quad -1 \quad -k_6 \quad -1 \quad k_6 \quad 1 \quad k_6)^t \\ k_6 &= \frac{b}{a}\end{aligned}\tag{3.8}$$

Stretching Mode:

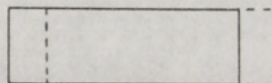
$$\begin{aligned}\lambda_7 &= \frac{b}{a} B + \lambda_p k_7 \\ \mathbf{v}_7 &= (1 \quad -k_7 \quad 1 \quad k_7 \quad -1 \quad k_7 \quad -1 \quad -k_7)^t \\ k_7 &= -\frac{1}{2} \left(\frac{b}{a} - \frac{a}{b} \right) \left(\frac{1-\nu}{\nu} \right) - \frac{1}{2} \sqrt{\left(\frac{b}{a} - \frac{a}{b} \right)^2 \left(\frac{1-\nu}{\nu} \right)^2 + 4}\end{aligned}\tag{3.9}$$

Extension Mode:

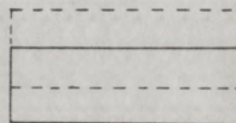
$$\begin{aligned}\lambda_8 &= \frac{b}{a} B + \lambda_p k_8 \\ \mathbf{v}_8 &= (1 \quad -k_8 \quad 1 \quad k_8 \quad -1 \quad k_8 \quad -1 \quad -k_8)^t \\ k_8 &= -\frac{1}{2} \left(\frac{b}{a} - \frac{a}{b} \right) \left(\frac{1-\nu}{\nu} \right) + \frac{1}{2} \sqrt{\left(\frac{b}{a} - \frac{a}{b} \right)^2 \left(\frac{1-\nu}{\nu} \right)^2 + 4}\end{aligned}\tag{3.10}$$

Note that the eigenvectors have been normalized such that their first non-zero term is unity. These modes are shown in Figure 7 for an element of aspect ratio 2.

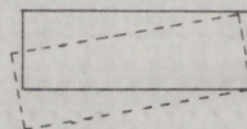
Rigid Body Mode (r direction):



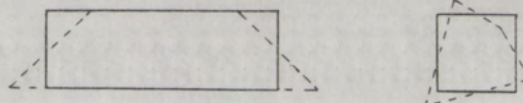
Rigid Body Mode (s direction):



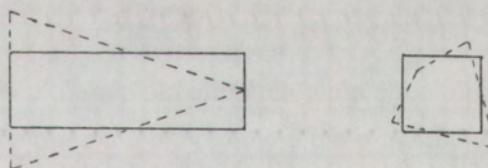
Rigid Body Mode (rotation):



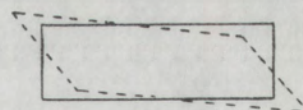
Flexure Mode 1:



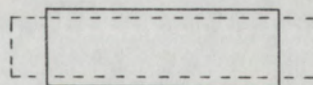
Flexure Mode 2:



Shear Mode:



Stretching Mode:



Extension Mode:

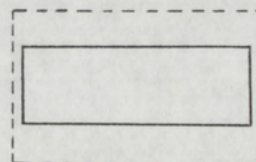


Figure 7. Mode Shapes

Notice that if $a = b$ (or if the aspect ratio $\frac{a}{b} = 1$), then the eigenvalues for the two flexure modes are equal. When this occurs, the two modes combine to give the following:

Flexure Mode 1:

$$\begin{aligned}\lambda_4 &= \frac{1}{3}(B + G) \\ \mathbf{v}_4 &= (1 \quad 1 \quad -1 \quad -1 \quad 1 \quad 1 \quad -1 \quad -1)^t\end{aligned}\tag{3.13}$$

Flexure Mode 2:

$$\begin{aligned}\lambda_5 &= \frac{1}{3}(B + G) \\ \mathbf{v}_5 &= (1 \quad -1 \quad -1 \quad 1 \quad 1 \quad -1 \quad -1 \quad 1)^t\end{aligned}\tag{3.14}$$

These latter two modes are also shown in Figure 7. Figures 8 and 9 show the variation in the eigenvalues with aspect ratio for a Poisson ratio of 0.25. The eigenvalues of two of the modes actually decrease for an aspect ratio that increases from one. The eigenvalue of the flexure mode 1 decreases to a minimum at an aspect ratio of 1.73 (for $\nu = 0.25$) while the stretching mode eigenvalue approaches zero for increasing aspect ratio.

The previous results are for an exactly or fully integrated stiffness matrix as defined by Equation (2.34). But how does underintegration affect these modes, since it has been seen to have a large effect on the calculated displacements?

It is interesting to note that underintegration affects only the two flexure modes. The eigenvalues associated with these modes are reduced and for an aspect ratio of one the eigenvectors are also changed. In this case, underintegration causes a shift from the eigenvectors given by Equations (3.13) and (3.14) to those given by Equations (3.6) and (3.7). The eigenvalues are summarized in Table 1 for the various integrations schemes. Note that the fully integrated values are simply sums of the contributions made separately by a full integration in each direction.

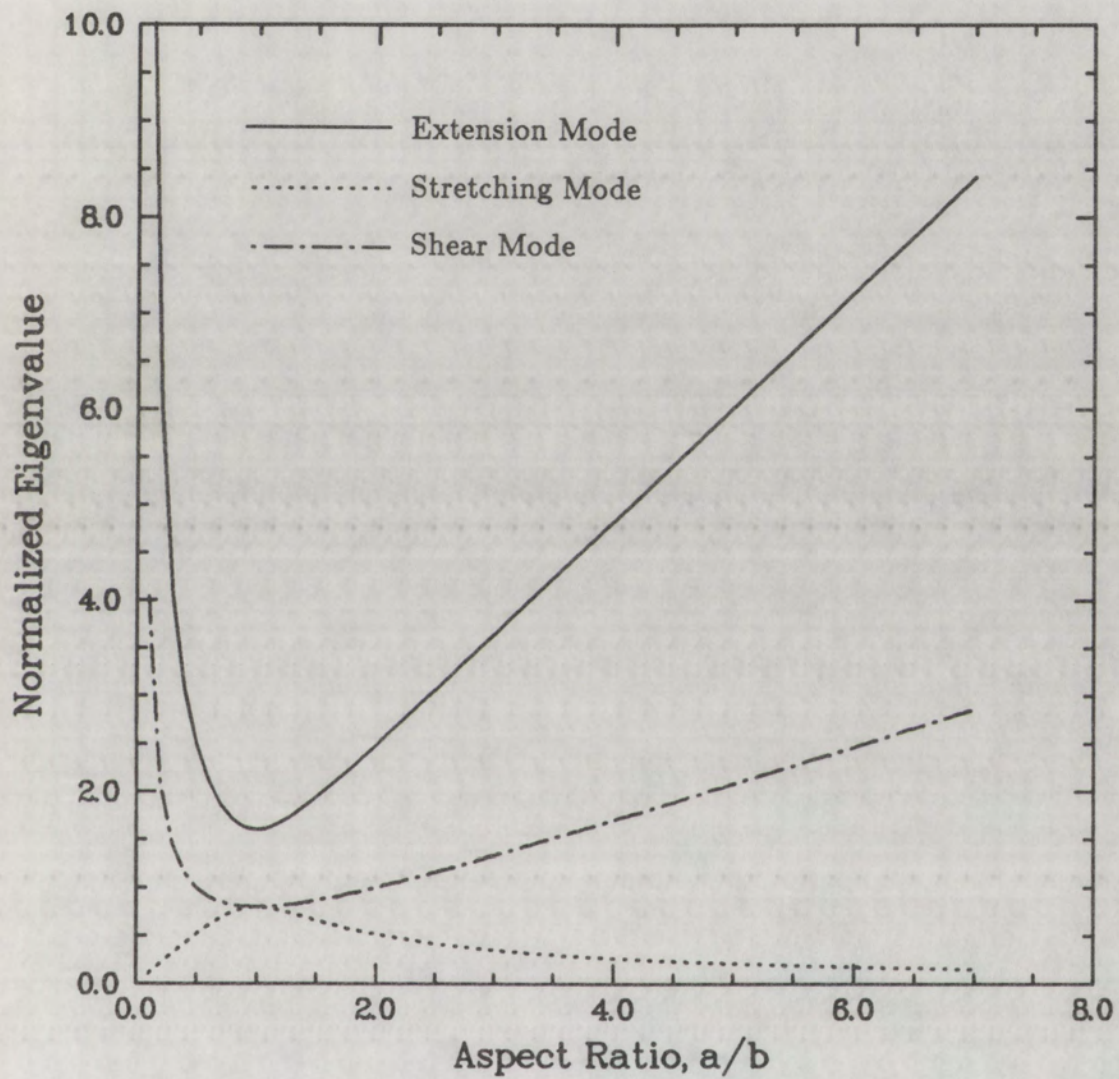


Figure 8. Shear, Stretching, and Extension Mode Eigenvalues

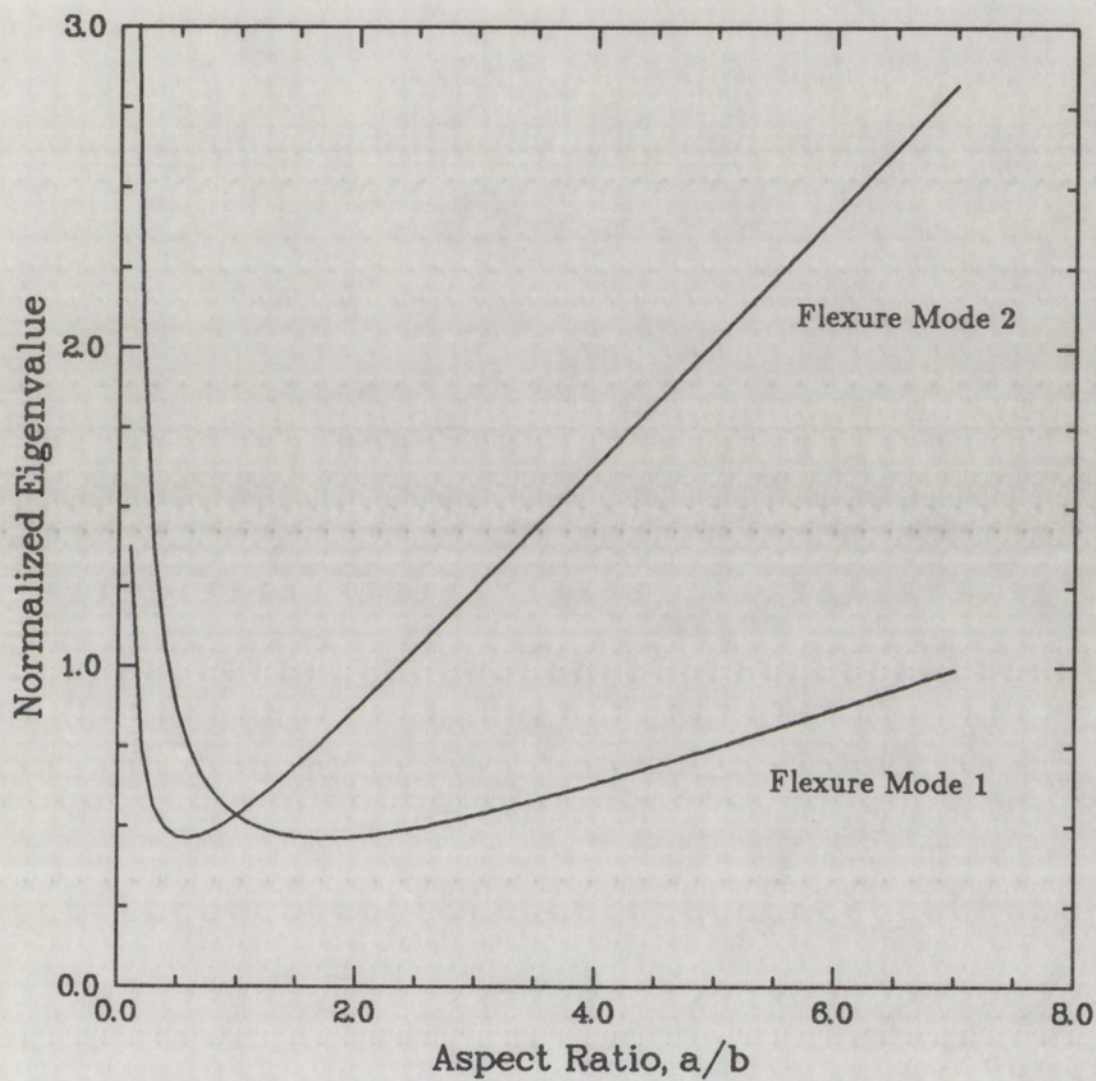


Figure 9. Flexure Mode Eigenvalues

Mode	2×2	2×1	1×2	1×1
Flexure 1	$\frac{1}{3}(\frac{b}{a}B + \frac{a}{b}G)$	$\frac{1}{3}\frac{a}{b}G$	$\frac{1}{3}\frac{b}{a}B$	0
Flexure 2	$\frac{1}{3}(\frac{a}{b}B + \frac{b}{a}G)$	$\frac{1}{3}\frac{a}{b}B$	$\frac{1}{3}\frac{b}{a}G$	0

Table 1. Flexure Mode Eigenvalues for Various Integrations

The eigenvalues resulting from a one-point integration are zero and thus the corresponding eigenvectors cause the hourglassing in dynamic problems. For this reason, the flexure modes are sometimes referred to as hourglass modes (and from this point on the two names are used interchangeably). If these modes are present in a given solution, it takes no energy to excite them and they may then dominate the solution. In static calculations, these zero eigenvalues are the cause of potential zero eigenvalues in the global stiffness matrix. The global stiffness matrix can still be nonsingular, however, if the boundary conditions are of such a type that the eigenvectors associated with zero eigenvalues are constrained. On the element level, since these are the only two modes to change, and since underintegration has been shown to "soften" a finite element system, then these are the modes that dictate the stiffness (in bending).

The flexure mode eigenvalues are plotted again in Figures 10 and 11 along with the corresponding eigenvalues for the 2×1 and 1×2 integrations. Notice that the two partial integrations serve as asymptotes to the full integrations. This is due the fact that the eigenvalues for the fully integrated case are the sums of the eigenvalues of the two partial integrations.

Further, the two flexure modes are the only ones affected by the reduced-selective integration procedure. Again, the eigenvalues are decreased from their fully integrated values. Table 2 compares the two flexure eigenvalues for full and reduced-selective integrations.

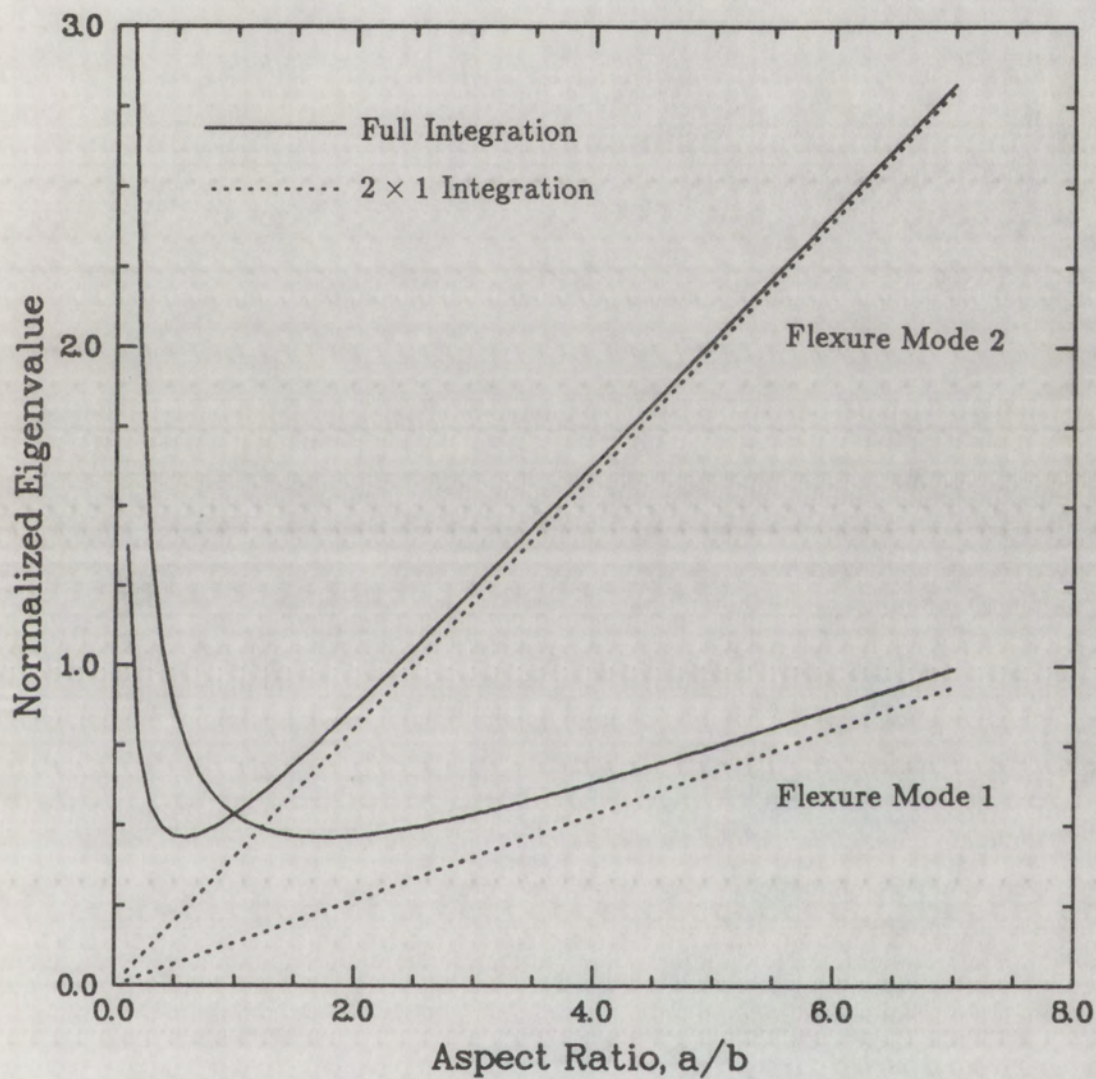


Figure 10. Flexure Mode Eigenvalues for Full and 2×1 Integrations

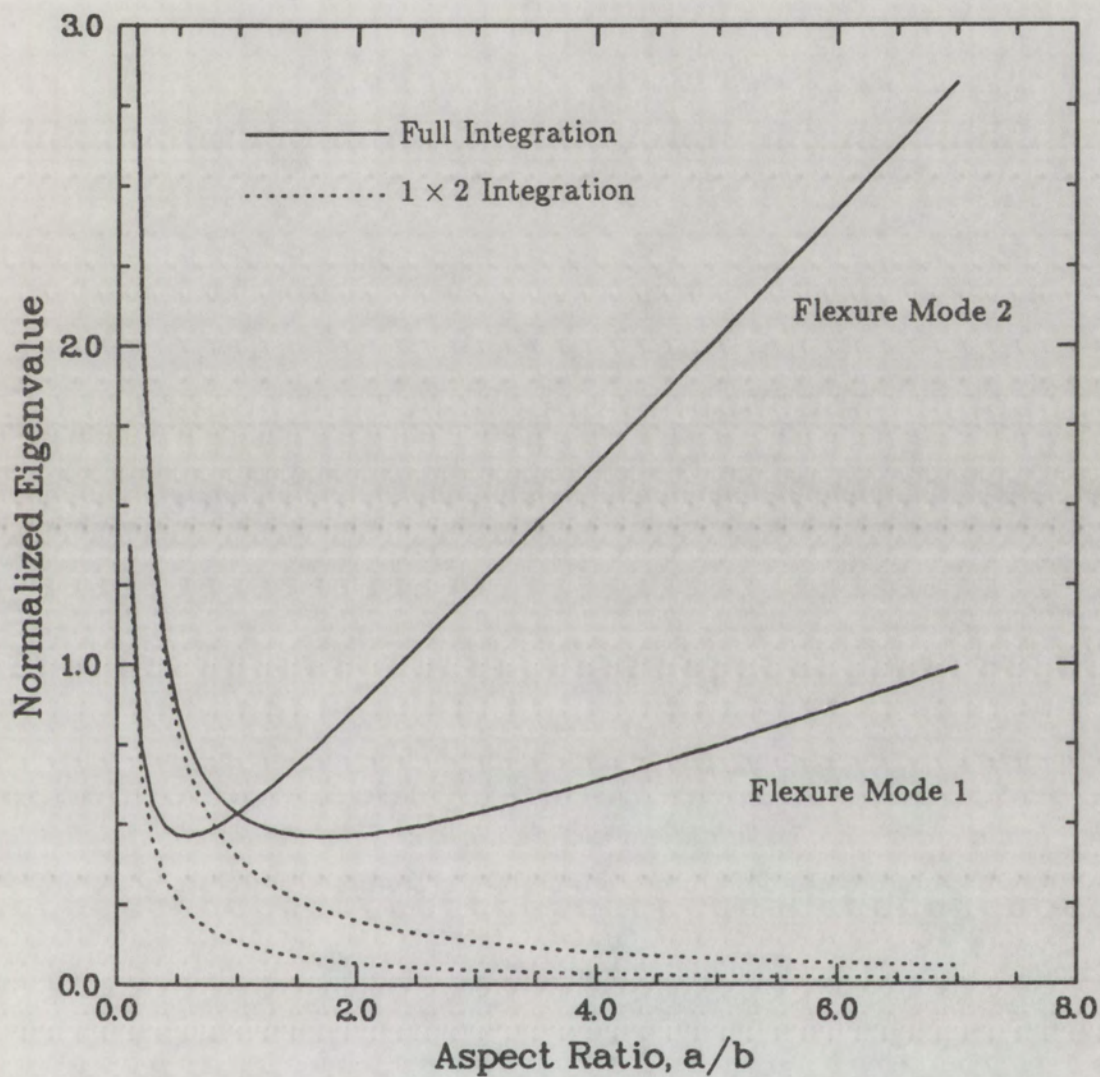


Figure 11. Flexure Mode Eigenvalues for Full and 1×2 Integrations

Mode	Full	Reduced-Selective
Flexure 1	$\frac{1}{3}(\frac{b}{a}B + \frac{a}{b}G)$	$(\frac{2}{3}\frac{b}{a} + \frac{1}{3}\frac{a}{b})G$
Flexure 2	$\frac{1}{3}(\frac{a}{b}B + \frac{b}{a}G)$	$(\frac{2}{3}\frac{a}{b} + \frac{1}{3}\frac{b}{a})G$

Table 2. Flexure Mode Eigenvalues for Full and
Reduced-Selective Integrations

The reason that reduced-selective integration works is most easily explained from an eigenvalue point of view. The fully integrated eigenvalues are made up of both volumetric and shear terms (the constrained modulus, B , is a volumetric term and approaches infinity as ν approaches 0.5). Reduced-selective integration removes the volumetric dependence and leaves only shear terms in the flexure mode eigenvalues. Thus the reduced-selective flexure eigenvalues remain finite for incompressible materials.

Figure 12 shows a comparison between the flexure eigenvalues for a full integration and the reduced-selective integration. When the dominant terms in the fully integrated eigenvalues contain the shear modulus G the reduced-selective eigenvalues approach the fully integrated case (i.e. flexure mode 1 for large aspect ratios). But when the fully integrated eigenvalues are dominated by the constrained modulus B , the reduced-selective values are significantly lower (flexure mode 2 for large eigenvalues). The behavior presented in Figure 12 represents the case of $\nu = 0.25$.

Again, underintegration has been shown to "soften" finite element systems but it also has the problems of hourglassing and singularities. In the case of reduced-selective integration, one matrix must still be fully integrated which takes more computer time and memory than a single point integration. It may thus be beneficial to formulate the element to be somewhere in between a full and a one-point integration. In this case the stabilization matrix becomes useful.

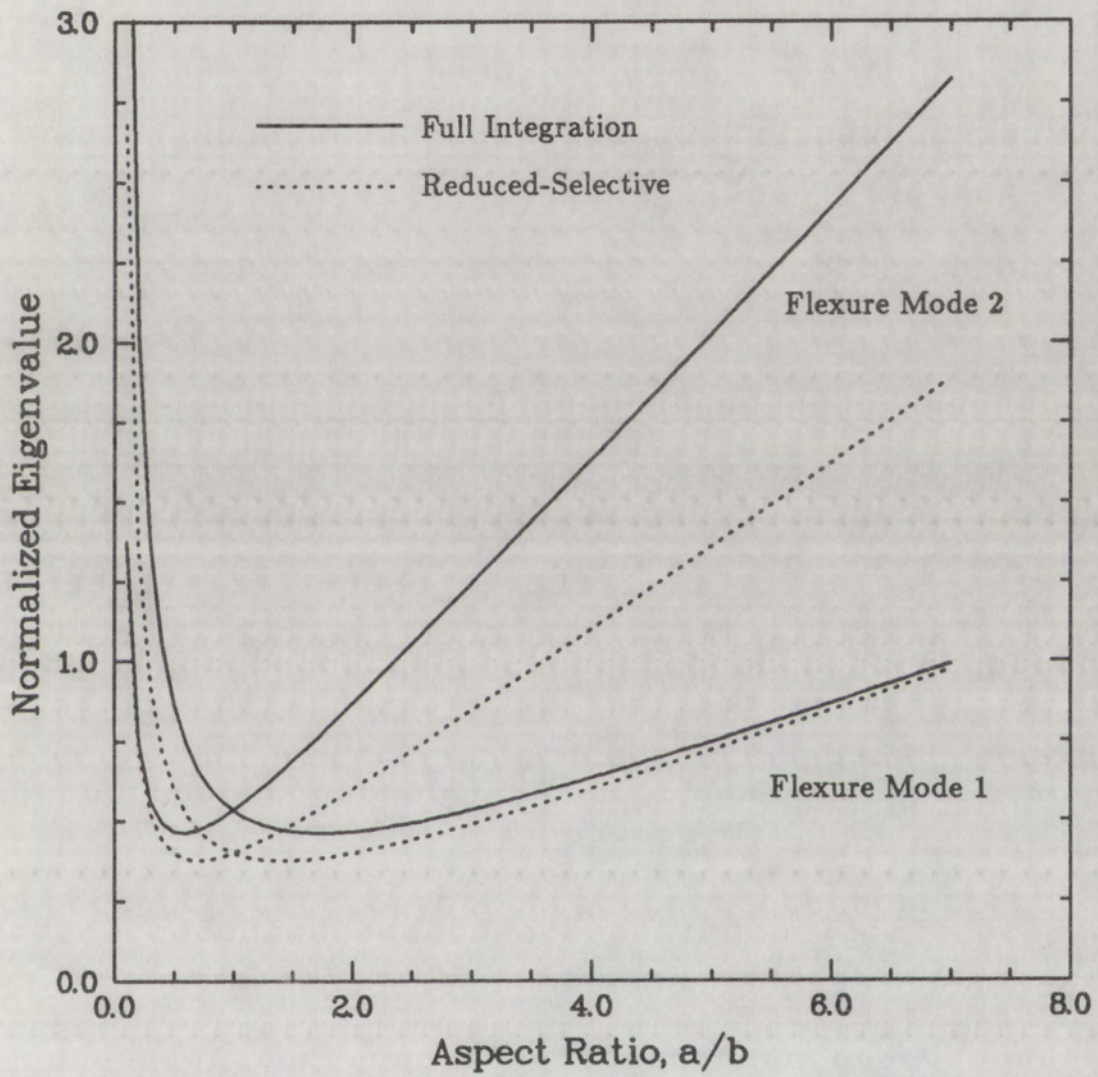


Figure 12. Flexure Mode Eigenvalues for Full and Reduced-Selective Integrations

IV. Stabilization Matrix

The stabilization matrix was defined by Belytschko *et al.* (1984) for the diffusion element to be

$$\mathbf{K}_{stab} = \bar{\epsilon} \gamma \gamma^t \quad (4.1)$$

where the vector γ was expressed in terms of the hourglass mode and the other modes of the element. The parameter $\bar{\epsilon}$ was normalized such that the stabilization matrix, when added to the conductance matrix (analogous to the stiffness matrix) as evaluated by one-point integration, would give the exact or fully integrated conductance matrix for a rectangular element

$$\mathbf{K}_{1pt} + \mathbf{K}_{stab} = \mathbf{K}_{full}. \quad (4.2)$$

The use of the stabilization matrix was then to control hourglassing in dynamic problems with $\bar{\epsilon}$ chosen to be some small value. This provides hourglass control that is orthogonal to the other modes in the problem, particularly the rigid body modes. Thus the hourglass control will not be activated in rigid body motion.

Jacquotte and Oden (1984) generalized somewhat the work by Belytschko *et al.* (1984) and derived a general integral form for $\bar{\epsilon}$ for non-parallelogram diffusion elements. They observed that for parallelogram elements the integral for $\bar{\epsilon}$ has a closed form solution (for skewed elements the integral must be evaluated numerically) and that γ reverts to the hourglass eigenvector. For the special case of rectangular elements, $\bar{\epsilon}$ is given as

$$\bar{\epsilon} = \frac{l_x^2 + l_y^2}{12l_x l_y} \quad (4.3)$$

where l_x and l_y are the lengths of the sides of the rectangular element. This is actually the hourglass mode eigenvalue divided by 4 for the rectangular diffusion element (the factor of 4 is not necessary when the hourglass eigenvector is normalized by setting its Euclidean norm equal to one). They have also suggested that a

more efficient way to obtain a "fully integrated" conductance matrix is to use the stabilization matrix. Then only one 2×2 integration (to evaluate $\bar{\epsilon}$) is necessary instead of 10 for the diffusion element.

In light of the findings summarized above for the diffusion element and since it has been shown in section III that only the hourglass/flexure modes change with the various integrations, it is reasonable to examine the exact contributions to the stiffness matrix of the element by these two modes. A modal decomposition of the stiffness matrix is performed to express the components of the matrix in terms of its eigenvalues and eigenvectors. This decomposition is shown below:

$$\mathbf{K} = \mathbf{M}\mathbf{\Lambda}\mathbf{M}^t. \quad (4.4)$$

The columns of the matrix \mathbf{M} are the eigenvectors and $\mathbf{\Lambda}$ is a diagonal matrix containing the eigenvalues. By examining the contributions of λ_4 and λ_5 the following relationship can be found:

$$\mathbf{K}_{full} = \mathbf{K}_{1pt} + \frac{1}{4}\lambda_4\mathbf{v}_4\mathbf{v}_4^t + \frac{1}{4}\lambda_5\mathbf{v}_5\mathbf{v}_5^t. \quad (4.5)$$

Substitution of Equation (4.5) into Equation (4.2) yields the following definition for the stabilization matrix:

$$\mathbf{K}_{stab} = \frac{1}{4}\lambda_4\mathbf{v}_4\mathbf{v}_4^t + \frac{1}{4}\lambda_5\mathbf{v}_5\mathbf{v}_5^t. \quad (4.6)$$

Thus the exact relationship between the stabilization matrix and the flexure modes has been defined. Remember that the two eigenvalues λ_4 and λ_5 can have very different values for elements of various aspect ratios, so the two parts of the stabilization matrix can have vastly different magnitudes. As with the diffusion element, the factors of 4 in Equations (4.5) and (4.6) would not be necessary if the eigenvectors \mathbf{v}_4 and \mathbf{v}_5 were normalized by setting their Euclidean norms equal to one. The components of the stabilization matrix are shown in Figure 13.

$$\begin{array}{cccccccc}
\frac{1}{4}\lambda_4 & 0 & -\frac{1}{4}\lambda_4 & 0 & \frac{1}{4}\lambda_4 & 0 & -\frac{1}{4}\lambda_4 & 0 \\
0 & \frac{1}{4}\lambda_5 & 0 & -\frac{1}{4}\lambda_5 & 0 & \frac{1}{4}\lambda_5 & 0 & -\frac{1}{4}\lambda_5 \\
-\frac{1}{4}\lambda_4 & 0 & \frac{1}{4}\lambda_4 & 0 & -\frac{1}{4}\lambda_4 & 0 & \frac{1}{4}\lambda_4 & 0 \\
0 & -\frac{1}{4}\lambda_5 & 0 & \frac{1}{4}\lambda_5 & 0 & -\frac{1}{4}\lambda_5 & 0 & \frac{1}{4}\lambda_5 \\
\frac{1}{4}\lambda_4 & 0 & -\frac{1}{4}\lambda_4 & 0 & \frac{1}{4}\lambda_4 & 0 & -\frac{1}{4}\lambda_4 & 0 \\
0 & \frac{1}{4}\lambda_5 & 0 & -\frac{1}{4}\lambda_5 & 0 & \frac{1}{4}\lambda_5 & 0 & -\frac{1}{4}\lambda_5 \\
-\frac{1}{4}\lambda_4 & 0 & \frac{1}{4}\lambda_4 & 0 & -\frac{1}{4}\lambda_4 & 0 & \frac{1}{4}\lambda_4 & 0 \\
0 & -\frac{1}{4}\lambda_5 & 0 & \frac{1}{4}\lambda_5 & 0 & -\frac{1}{4}\lambda_5 & 0 & \frac{1}{4}\lambda_5
\end{array}$$

Figure 13. Components of Element Stabilization Matrix

For hourglass control in dynamic problems, only a portion of the stabilization matrix is used with the one-point stiffness matrix to define a total stiffness matrix. Thus, the matrix \mathbf{K} is expressed as

$$\mathbf{K} = \mathbf{K}_{1pt} + \bar{\mathbf{K}}_{stab} \quad (4.7)$$

where

$$\bar{\mathbf{K}}_{stab} = \frac{1}{4}\bar{\epsilon}_4\lambda_4\mathbf{v}_4\mathbf{v}_4^t + \frac{1}{4}\bar{\epsilon}_5\lambda_5\mathbf{v}_5\mathbf{v}_5^t. \quad (4.8)$$

or

$$\bar{\mathbf{K}}_{stab} = \frac{1}{4}\bar{\lambda}_4\mathbf{v}_4\mathbf{v}_4^t + \frac{1}{4}\bar{\lambda}_5\mathbf{v}_5\mathbf{v}_5^t. \quad (4.9)$$

where $\bar{\lambda}_4$ and $\bar{\lambda}_5$ are arbitrarily chosen values. The reason is that, in general, exact values for these eigenvalues are unknown so suitable values have been chosen by trial and error. For rectangular elements, exact values are now available as given in Equations (3.6) and (3.7).

As mentioned before, the choice of $\bar{\epsilon}$ (or $\bar{\lambda}$) is not well defined but as shown by Belytschko *et al.* (1984) for a dynamic beam problem and as will be seen in the next section for a static beam problem these alternative choices for values (of $\bar{\epsilon}$ or $\bar{\lambda}$) can drastically affect the peak displacements.

V. Numerical Results

It is well known that full integration of four node quadrilateral elements yields a system that is too stiff in its response to simple bending. As mentioned before, various schemes have been shown to provide improvement in the response of the element but often parameters are chosen merely by trial and error. In the stabilization procedure discussed above the aspect ratio is usually disregarded and the eigenvalues for each of the flexure modes are chosen to be the same. But now the exact expressions for the two eigenvalues are available and the stabilization procedure has been formulated with these expressions. With this information, various schemes were tried in which reduced eigenvalues were used to obtain both a more flexible response and no locking for nearly incompressible materials.

To evaluate two of the schemes that appeared the most promising, the problem of a tip loaded cantilever beam was analyzed. Rectangular elements of various aspect ratios were used to model the problem and Poisson's ratio was varied to assess the effect of nearly incompressible materials. The parameter used to gauge the performance of the schemes was the maximum tip deflection divided by the exact deflection as given by elementary beam bending theory.

Figure 14 shows a cantilever beam of dimensions $5 \times 1 \times 1$ subjected to a tip load of unit magnitude which was used as a test problem. Six sets of calculations

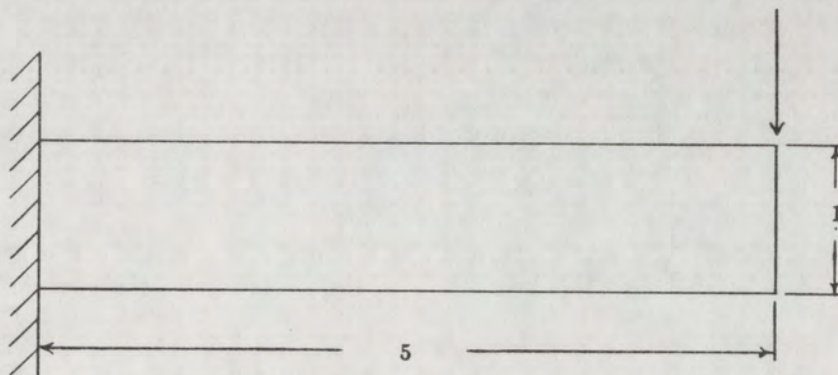


Figure 14. Cantilever Beam Problem

were performed in which tip displacements were generated for full integration, reduced-selective integration, and methods 1 and 2 presented below. Each set maintained a constant aspect ratio (aspect ratios of 1, 2.5, and 5 were tested) and a constant Poisson's ratio (0.25 and 0.45 were used). Young's modulus of one was used throughout. The mesh used for each set started out with only one element through the thickness and either one, two or five elements along the length of the beam. These meshes were refined by doubling the number of elements along the length and through the thickness so that the same aspect ratio was maintained with mesh refinement. The two most promising methods (arrived at by trial and error) for choosing the flexure eigenvalues for use in Equation (4.9) are shown below:

Method 1:

$$\bar{\lambda}_4 = (0.9)\left(\frac{1}{3}\frac{b}{a}B\right) \quad (5.1)$$

$$\bar{\lambda}_5 = (0.9)\left(\frac{1}{3}\frac{a}{b}B\right) \quad (5.2)$$

Method 2:

$$\bar{\lambda}_4 = \left((0.9)\frac{b}{a} + (0.005)\frac{a}{b}\right)G \quad (5.3)$$

$$\bar{\lambda}_5 = \left((0.9)\frac{a}{b} + (0.005)\frac{b}{a}\right)G \quad (5.4)$$

These methods were patterned after a partial integration and a reduced-selective integration. Care was taken to ensure that the eigenvalue of flexure mode 2 at an aspect ratio of $\frac{b}{a}$ was the same as that of flexure mode 1 at an aspect ratio of $\frac{a}{b}$ (and thus the eigenvalues are equal at an aspect ratio of one). This was done so that the problem could be oriented in either the x or the y directions. With these new methods, however, comes the possibility that monotonic convergence of the element will be lost. For this reason, the calculations were conducted in such a manner that the number of elements used in the problem was increased in the same way that standard convergence studies are performed.

Plotted in Figure 15 are the normalized tip displacements (u_{fem}/u_{exact}) versus number of elements used in the mesh for elements with an aspect ratio of 1 and ν equal to 0.25. The full integration results in a much stiffer system than the other three methods. While reduced-selective integration yields a more flexible system, results of methods 1 and 2 come closest to a normalized displacement of 1.

Figure 16 presents the same information for an aspect ratio of 2.5. The results for all four methods are lower but the full and the reduced-selective integration displacements are closer to one another and have dropped drastically. Methods 1 and 2 remain within 12% of the exact solution even for a two element mesh. Figure 17 indicates that this trend continues for an aspect ratio of 5.

Figures 18 through 20 show similar results for the three aspect ratios when ν is 0.45. For an aspect ratio of one (Figure 18), full integration and method 1 give stiffer results for $\nu = 0.45$ as compared to $\nu = 0.25$ as expected. Reduced-selective integration and method 2, however, give results that are too flexible. The displacements actually decrease with increasing number of elements.

Figure 19 shows that only method 2 is too flexible for an aspect ratio of 2.5. But after an initial decrease, the displacements for this method increase toward the exact solution. Figure 20 is similar except that method 2 normalized displacements now remain less than one (but there is still an initial decrease).

The decreasing displacements for reduced-selective integration and method 2 in Figures 18 through 20 indicate that the number of elements used through the thickness of the beam can have a large effect. The initial drop occurs in going from one element to two elements through the beam thickness. The explanation for this behavior is that as the number of elements through the thickness is increased, the bending response of the system becomes less dependent on the element flexure modes. When only one element is used, bending of the beam occurs only through the element flexure modes. With many elements through the thickness, the stretching

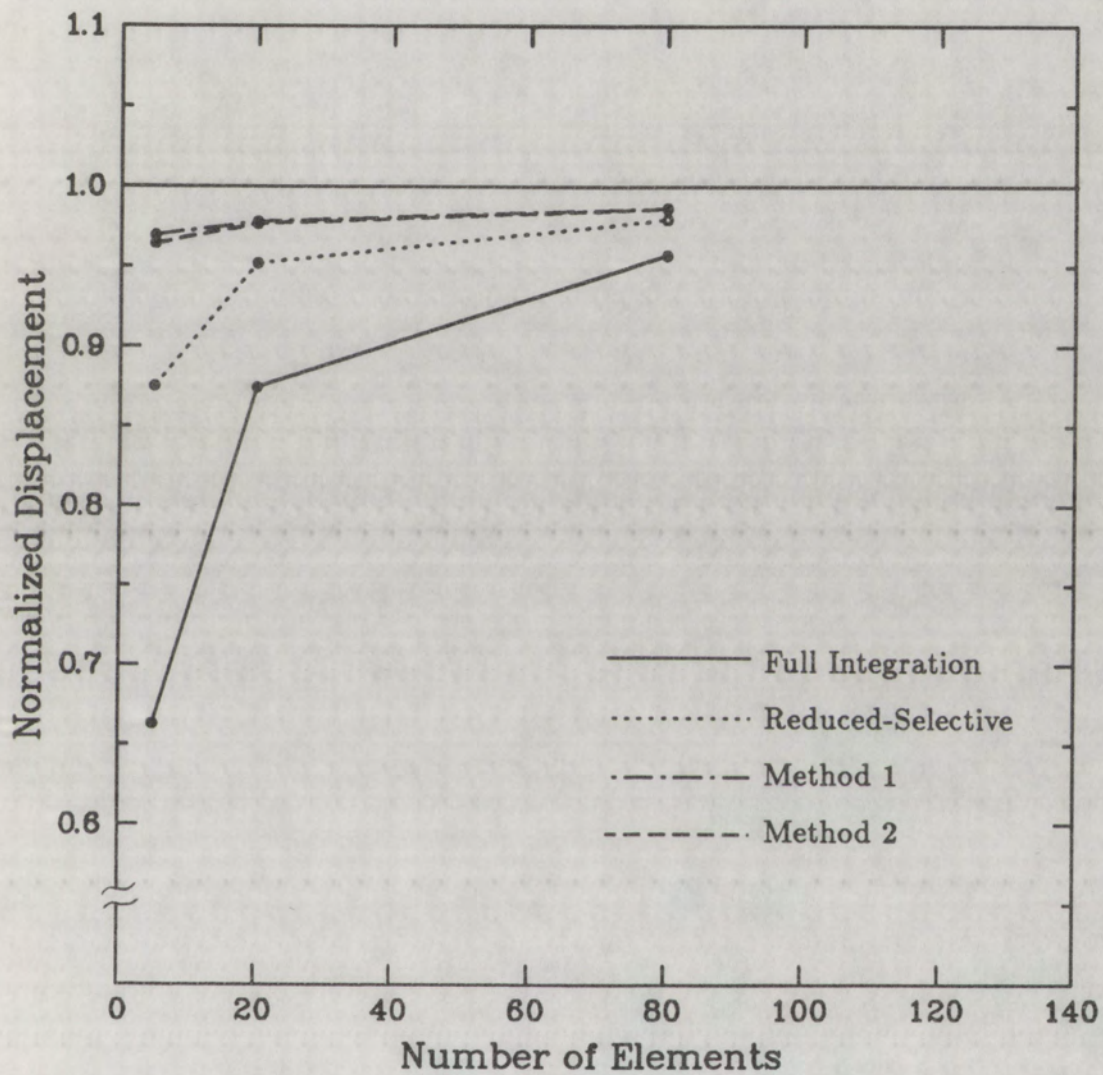


Figure 15. Normalized Tip Displacements

$$\frac{a}{b} = 1, \nu = 0.25$$

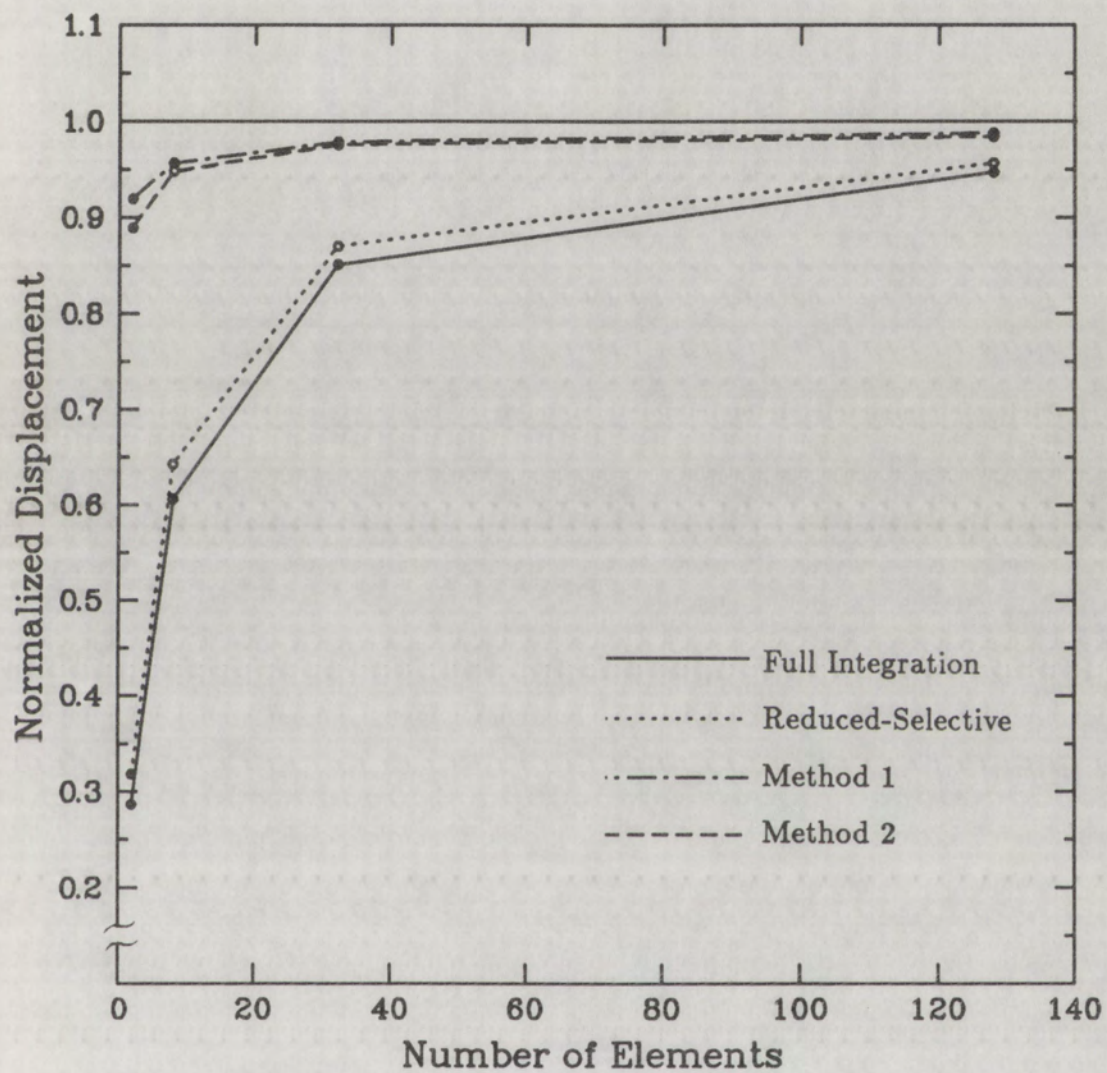


Figure 16. Normalized Tip Displacements

$$\frac{a}{b} = 2.5, \nu = 0.25$$

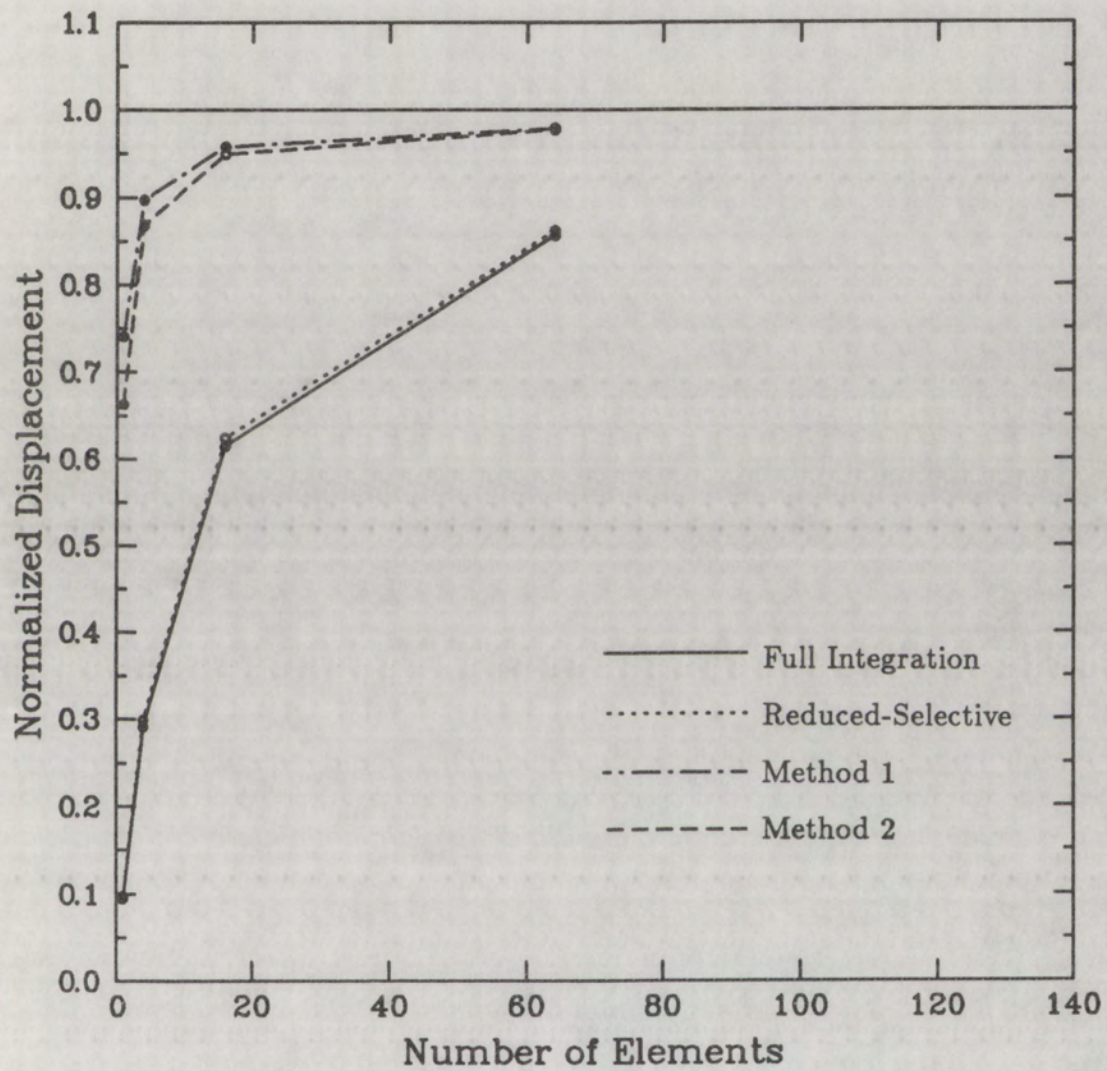


Figure 17. Normalized Tip Displacements

$$\frac{a}{b} = 5, \nu = 0.25$$

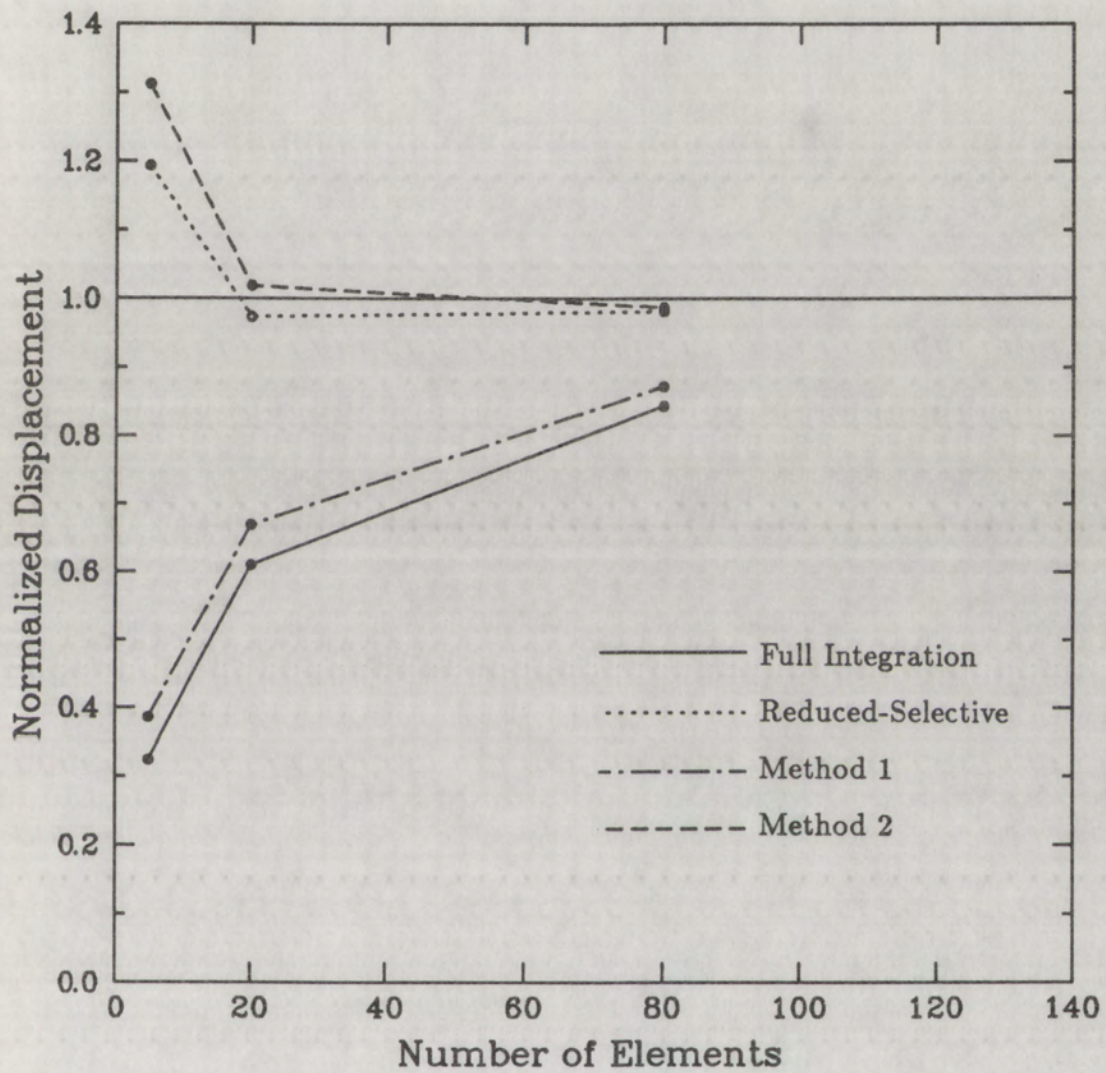


Figure 18. Normalized Tip Displacements

$$\frac{a}{b} = 1, \nu = 0.45$$

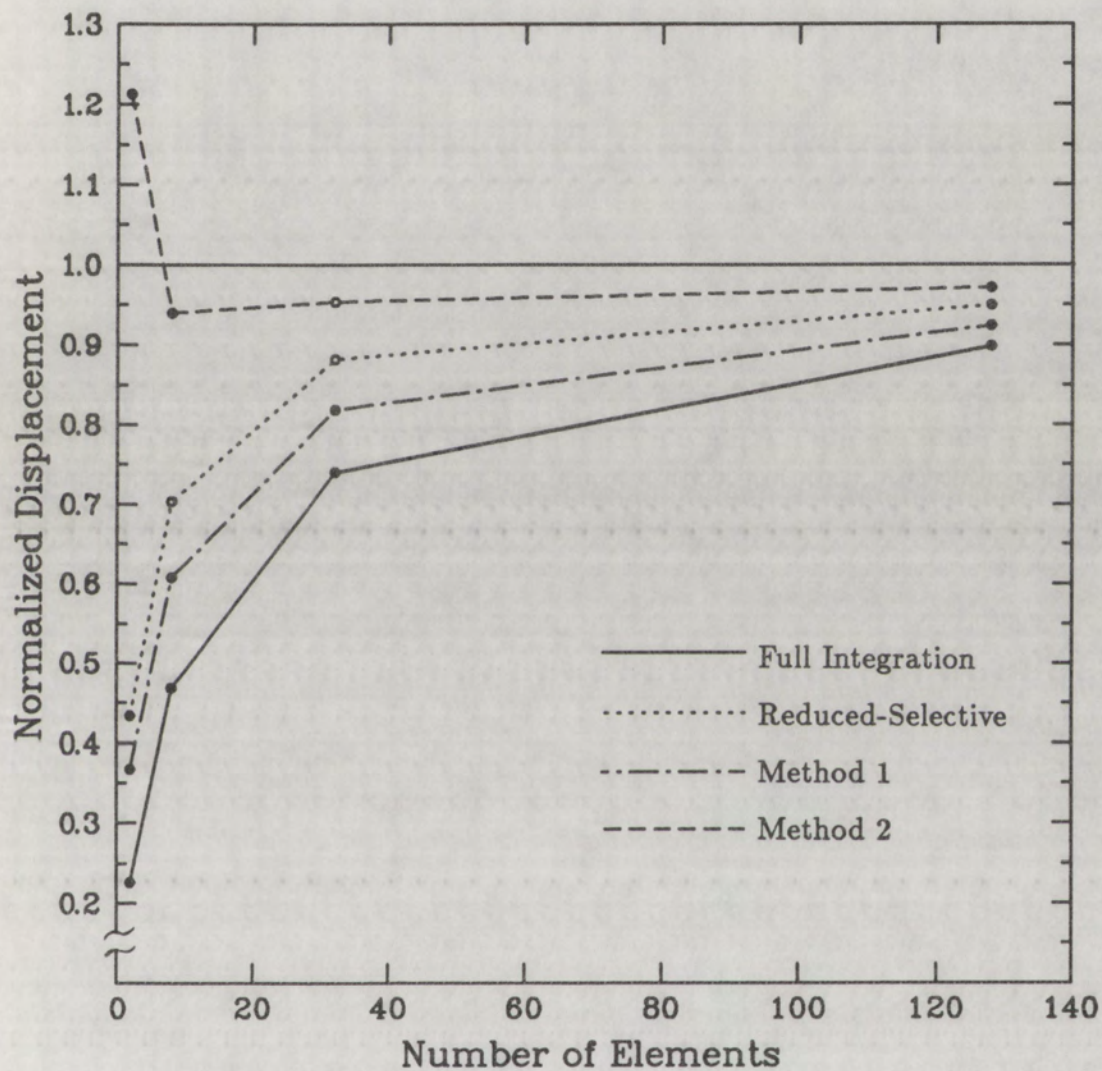


Figure 19. Normalized Tip Displacements

$$\frac{a}{b} = 2.5, \nu = 0.45$$

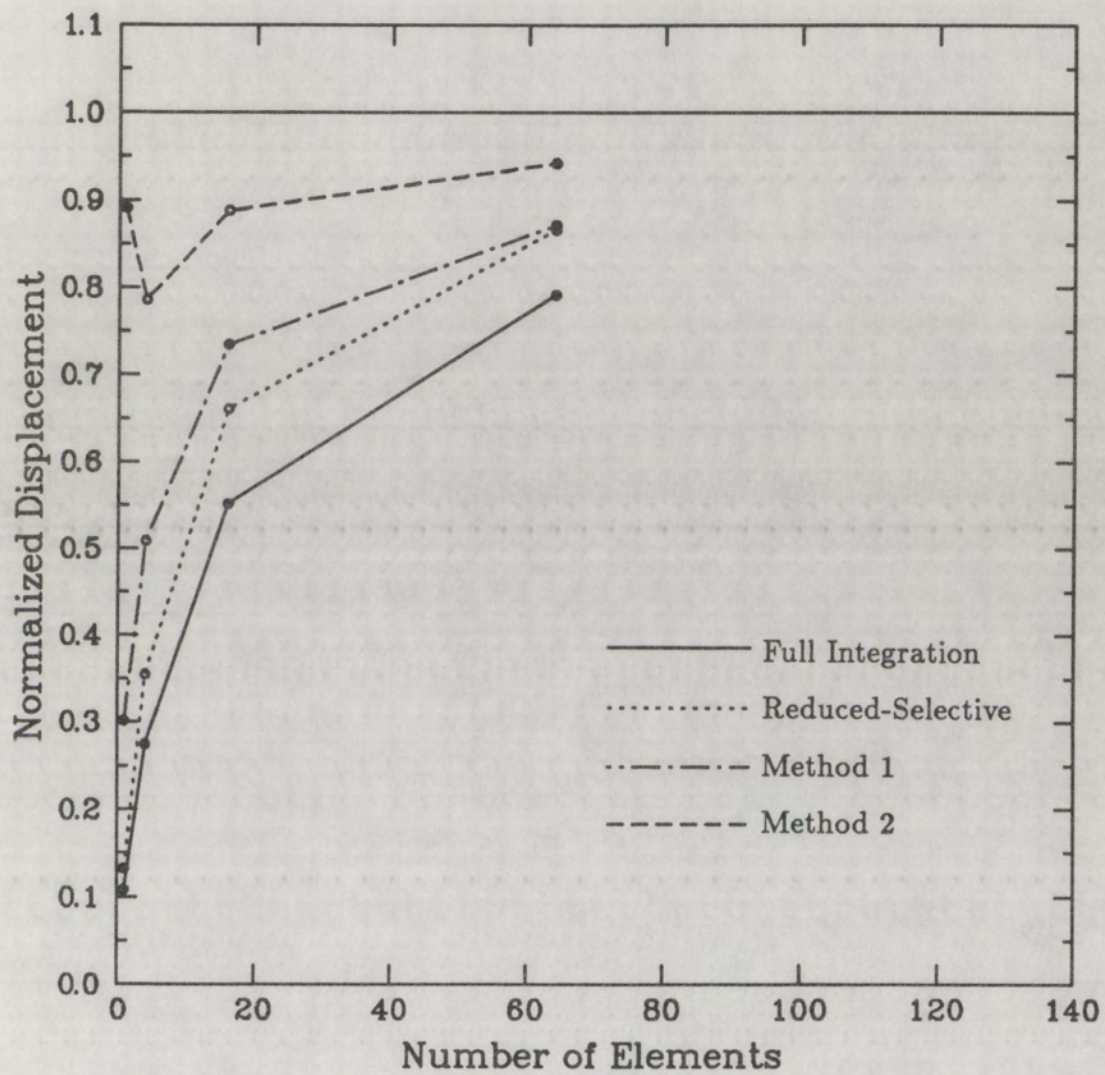


Figure 20. Normalized Tip Displacements

$$\frac{a}{b} = 5, \nu = 0.45$$

and extension modes dominate the bending response because of the tensile and compressive stresses on either side of the neutral axis. By adjusting method 2 to provide some degree of flexibility in meshes with several elements through the beam thickness and since the method accounts only for changes in element aspect ratio, the flexure eigenvalues it yields are too small when the thickness is modelled with only one element.

It has been noted in the course of this study that the dominant mode of the element in bending is the flexure mode 1. This seems obvious from the shape of the mode, but it is also born out by the numerical results. Refer again to Figure 12 and note that the eigenvalue of flexure mode 1 for reduced-selective integration approaches that for a full integration as the aspect ratio increases, and that the corresponding eigenvalues of flexure mode 2 diverge. Now note that the results in Figures 15 through 20 are most different between these two integrations for an aspect ratio of 1 and become closer for increasing aspect ratio. Therefore, flexure mode 1 has a stronger effect on the displacements than does flexure mode 2.

The additional stiffness approach proposed by Prathap (1985) and presented in Equations (2.37) through (2.39) was also investigated. The additional stiffness parameter e_{fem} was calculated using the tip displacement at the neutral axis for the beam problem of Figure 14. The stiffness parameters are compared in Table 3 (ν is equal to 0.25 and 5 elements are used to model the length of the beam). The fully integrated finite element results followed the predicted trend that the stiffest result occurs for one element through the thickness of the beam and the displacements then approach some bounding value as the number of elements used through the thickness is increased. Agreement with Prathap's work is quite good; for 8 elements through the thickness the tip displacement comes to within 1.5% of that predicted for an "infinite" number of elements.

	Number of Elements through Beam Thickness					
	1	2	4	6	8	∞
e_{fem}	0.51	0.43	0.41	0.41	0.40	—
e_1	0.50	—	—	—	—	—
e_∞	—	—	—	—	—	0.38

Table 3. Additional Stiffness Parameters

VI. Conclusions

This thesis has shown various causes of and remedies for the excessively stiff behavior exhibited in bending by the four node plane stress/plane strain quadrilateral finite element. The response of the element has been described as a function of its aspect ratio and material properties through the use of its eigenvalues and eigenvectors. It has been shown that the two flexure modes of the element dominate the bending response with flexure mode 1 being the more important of the two.

With the functional form of the eigenpairs and knowing how they change with various integrations, the element behavior is more clearly understood. It was seen how locking occurs for incompressible materials because the eigenvalues associated with the flexure modes become infinite. Further, it was shown how underintegration (and reduced-selective integration) "unlocks" the element by reducing the eigenvalues (or for incompressible materials by keeping the eigenvalues finite). Also the zero eigenvalues caused by a one-point integration can lead to singularities in the global stiffness matrix that can cause hourglassing in dynamic problems or preclude a static solution for certain boundary conditions.

The stiffness due to aspect ratio seems to be related more to the eigenvectors than the eigenvalues. Flexure mode 1, the dominant flexure mode, has an eigenvalue that changes only slightly with the aspect ratio (in comparison to the other modes). This mode allows bending type displacements to occur only at the ends of the element (refer to Figure 7). If the eigenvalue is approximately the same for an element of two different aspect ratios then the actual displacements will be similar but the displacement per unit length will be lower for the longer element. Thus the aspect ratio stiffness appears to be caused by the shape of the dominant flexure eigenvector.

The stabilization matrix formulation was found to provide a convenient method by which the element response can be adjusted. By reducing the flexure eigenvalues

in a certain way the response was seen to be more flexible. However, care must be taken to ensure that convergence is not lost.

The approach that this study has taken to investigate poor element response has been seen to work quite well. It has led to a better understanding of the element, its uses, and shortcomings. A logical extension of this work is to apply the approach to elements of irregular geometry. A more general geometry parameter (or parameters) would have to be defined and determination of the eigenpairs would have to be done numerically. But this could still give an indication as to an appropriate method for choosing stabilization matrix components for improved element response.

Also, since it has been seen that modes other than the flexure modes can contribute significantly to the bending stiffness of the system, another extension of this work could be to investigate methods to adjust all of the eigenvalues of the element. A possible technique to accomplish this is to choose the eigenvalue of a mode based on the minimum strain energy of the mode. The minimum energy of a mode would be determined by applying the nodal displacements of the eigenvector to a volume element and allowing the volume element to take a shape that gives the minimum strain energy. The resulting displacement field is likely to be other than bilinear (which is the field prescribed by the finite element shape functions) and thus the new eigenvalue would likely be smaller.

References

- Bathe, K.J., 1982, *Finite Element Procedures in Engineering Analysis*, Prentiss-Hall, Englewood Cliffs, NJ, 169.
- Belytschko, T., Ong, J.S.-J., Liu, W.K., and Kennedy, J.M., 1984, "Hourglass Control in Linear and Nonlinear Problems", *Computer Methods in Applied Mechanics and Engineering*, vol. 43, 251-276.
- Flanagan, D.P., and Belytschko, T., 1981, "A Uniform Strain Hexahedron and Quadrilateral with Orthogonal Hourglass Control", *International Journal for Numerical Methods in Engineering*, vol. 17, 679-706.
- Jacquotte, O.-P., and Oden, J.T., 1984, "Analysis of Hourglass Instabilities and Control in Underintegrated Finite Element Methods", *Computer Methods in Applied Mechanics and Engineering*, vol. 44, 339-363.
- MacNeal, R.H., and Harder, R.L., 1985, "A Proposed Standard Set of Problems to Test Finite Element Accuracy", *Finite Elements in Analysis and Design*, vol. 1, 3-20.
- Prathap, G., 1985, "The Poor Bending Response of the Four-Node Plane Stress Quadrilateral", *International Journal for Numerical Methods in Engineering*, vol. 21, 825-835.
- Schulz, J.C., 1985, "Finite Element Hourglassing Control", *International Journal for Numerical Methods in Engineering*, vol. 21, 1039-1048.
- Zienkiewicz, O.C., 1977, *The Finite Element Method*, Third Edition, McGraw-Hill, London, 284-287.